

Systematic analysis of search strategies for $L_\mu - L_\tau$ gauge bosons at Belle II

Connor Brown^a, Juri Fiaschi^{a,b}, Oliver Fischer^a, Thomas Teubner^a

^a*Department of Mathematical Sciences, University of Liverpool, Liverpool L69 3BX, United Kingdom*

^b*Università degli Studi di Milano-Bicocca, Department of Physics “Giuseppe Occhialini”, & INFN, Sezione di Milano-Bicocca, Piazza della Scienza 3, Milano 20126, Italy*

E-mail: connor.brown@liverpool.ac.uk, juri.fiaschi@unimib.it,
oliver.fischer@liverpool.ac.uk, thomas.teubner@liverpool.ac.uk

ABSTRACT: Extensions of the Standard Model with masses at or below the GeV scale are motivated by searches for dark matter and precision measurements in the quark and lepton flavour sectors, including that of the muon anomalous magnetic moment. An excellent experimental environment to test such light new physics is given by the Belle II experiment, which foresees to take up to 50 ab^{-1} of data. Here we consider a model with an additional gauged $U(1)_{L_\mu - L_\tau}$ symmetry that introduces a neutral gauge boson, a Dark Photon, with possibly large couplings to muon- and tau-flavored leptons, including neutrinos. Dark Photon mixing with the Standard Model photon is loop induced, allowing it to couple to electrically charged fermions other than muons and taus. We systematically investigate the possible search strategies for Dark Photons with four fermion final states. We identified search channels with muons as the most promising ones, and we analyse the kinematic distributions to obtain cuts that optimise the sensitivity of Belle II searches for the Dark Photon. Summarising the sensitivities from the most promising search channels we provide a comprehensive overview of future searches at Belle II.

KEYWORDS: New Light Particles, Specific BSM Phenomenology, Dark Matter at Colliders

Contents

1	Introduction	1
2	Dark Photon Model and Decays	3
3	Dark photon signatures at Belle II	5
4	Analysis setup	8
5	Dark photon search channels	9
5.1	Monophoton	9
5.2	Two muons plus missing energy	13
5.3	Four muons prompt	14
5.4	Displaced vertices	18
5.5	Signatures with tau leptons	21
6	Results	22
7	Conclusions	25

Contents

1 Introduction

The Standard Model (SM) of particle physics is a remarkably successful theory, thoroughly tested by many experiments in the past decades. The theory appears incomplete as it is unable to explain numerous phenomena - such as the existence of dark matter, the baryon asymmetry of the universe, and neutrino masses - while the increasing precision of modern measurements has revealed significant tensions - as the recent measurements of $g - 2$, the muon anomalous magnetic moment, at Fermilab [1–3], or the measurement of the W -boson mass by the CDF collaboration at the Tevatron [4]. New physics below the electro-weak (EW) scale, coupling very weakly to the SM, could solve tensions between SM predictions and experimental observations, including anomalies in the flavour sector. Importantly, new light states, which are singlet under the SM gauge group, can play the role of portals to hidden or dark sectors, hence connecting ordinary and dark matter.

A minimal extension of the SM, connecting the visible to a dark sector, can be constructed by adding an $U(1)_X$ Abelian gauge group which mixes with the SM $U(1)_Y$ hypercharge field [5]. The $L_\mu - L_\tau$ gauge symmetry is a popular choice for the new Abelian group, as it naturally predicts a small kinetic mixing with the SM neutral gauge bosons,

while keeping the theory renormalisable and anomaly free [6]. Such lepton non-universal interactions could also - at least partially - account for the discrepancy between theory [7, 8] and measurements [1, 2] of the muon anomaly. Currently, the status of the $g - 2$ discrepancy is unclear, due to significant tensions between data used in [7] as input in the data-driven evaluation of the hadronic vacuum polarisation contributions to $g - 2$ and the recent two-pion data from CMD-3 [9, 10], and due to tensions with the lattice predictions, in particular from the BMW collaboration [11]. However, with a lot of efforts on new and improved low-energy hadronic cross section measurements and on further lattice determinations, the comparison between the $g - 2$ measurement and its SM prediction is expected to be consolidated and could still indicate a significant discrepancy, or, in turn, strongly constrain physics beyond the SM.

Neutral vector bosons with masses below the GeV scale, generally called Dark Photons (DPs), can be probed looking at final states involving photons and leptons [12]. Experiments at colliders provide the strongest constraints for DP masses in the MeV to GeV range [13]. The LHC main experiments have performed dedicated DP searches, see e.g. LHCb [14, 15], ATLAS [16, 17], CMS [18–21]. However, due to the leptophilic nature of the $L_\mu - L_\tau$ symmetry, lepton colliders present unique opportunities to test this model. Because of the vanishing DP tree-level couplings to coloured particles, purely leptonic final states with high multiplicity are the most promising channels for investigating this model. In order to probe very low couplings, high intensity beams are needed to produce DPs at a detectable rate. High luminosity experiments like BaBar [22, 23], KLOE [24], Belle [25] and Belle II [26, 27] at the meson factories DAΦNE, PEP-II and KEK, are able to collect very large data samples, hence providing the highest sensitivity for $L_\mu - L_\tau$ DPs.

The DP associated with the $U(1)_{L_\mu - L_\tau}$ symmetry group can also act as a portal to a dark sector through its direct couplings to new invisible light states, such as dark chiral fermions or sterile/Majorana right-handed neutrinos, which can (at least partially) account for the observed dark matter relic abundance. DP portals to dark sectors have been probed through signatures with missing energy at lepton colliders (BaBar [28]) and beam dump experiments (E137 [29], NA64 [30]), or through their interactions with neutrinos (in neutrino trident production [31], at LSND [32], CHARM-II [33], CCFR [34], Borexino [35]) and dark matter (XENON [36, 37]) in scintillator and direct detection experiments. Dark matter coupled to the DP carries complementary constraints [38] from astrophysics and cosmology [39–42] as well as indirect detection (FERMI-LAT [43]) surveys.

Light DPs weakly coupled to the SM naturally feature macroscopic decay lengths, which lead to detectable displaced decay vertices. This is the case if the DP has a narrow width, which still holds in models where the DP acts as a portal to an extended dark sector, as long as the dark particles are heavy enough and any additional decay channels for the DP are kinematically forbidden. Signatures with displaced vertices represent a smoking gun for the discovery of long-lived particles. A very active ongoing programme at the LHC focuses on improving the sensitivity on long-lived particles [44–47], also exploiting the CERN Super Proton Synchrotron beam dump (NA64++ [48–50], NA48/2 [51]), the muon beam (MUonE [52]), or novel dedicated forward detectors (FASER [53–55], MATHUSLA [56, 57], CODEX-b [58]).

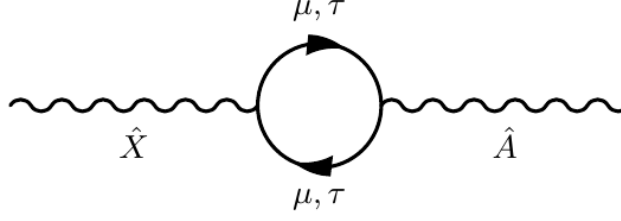


Figure 1. Loop induced mixing of the dark photon \hat{X} with the SM photon \hat{A} .

Similarly, dedicated searches for displaced signatures at lepton colliders [59] have been pursued by the KLOE [60], BaBar [23, 61], and Belle II [62–67] experiments. In the future, the light long-lived DP scenario can be best tested in the clean environment of e^+e^- collisions with the Belle II detector. Thanks to its large acceptance and with the prospect of high luminosity in the forthcoming years, we can expect a statistically significant sample to study long-lived DP signatures. The high energy asymmetric e^+e^- collisions generate a boost of the centre-of-mass frame, enhancing the lifetime of the final state system and the probability to observe events with a displaced decay vertex. The recast of the experimental displaced vertices search in the DP framework therefore provides a powerful probe to rule out yet unexplored regions in the parameter space for such BSM scenarios.

In this paper we consider the sensitivity of the Belle II target luminosity on the minimal BSM construction featuring a DP from an additional $U(1)_{L_\mu-L_\tau}$ gauge group, connected to the SM through kinetic mixing generated at loop-level. In Sect. 2 we introduce the DP model and its phenomenological key aspects, and discuss existing constraints. In Sect. 3 we assess the potential of DP searches at Belle II, with detailed analyses of the relevant signatures involving the new light neutral boson, including displaced vertex searches for long-lived DPs. In Sect. 6 we project the sensitivity of the ultimate Belle II target luminosity on the parameter space of the model, and compare it with the existing constraints. Finally, in Sect. 7 we draw our conclusions.

2 Dark Photon Model and Decays

We introduce a minimal BSM construction extending the SM gauge group with the local abelian group $U(1)_{L_\mu-L_\tau}$, with L_α being the lepton number of flavour α [68]. The corresponding gauge boson \hat{X}^μ interacts with the SM lepton current $j_\mu^{L_\mu-L_\tau}$, i.e. with the SM muon and tau charged and neutral leptons. The effective Lagrangian after EW symmetry breaking contains the terms

$$\mathcal{L} \supset -\frac{1}{4}\hat{F}_{\mu\nu}\hat{F}^{\mu\nu} - \frac{1}{4}\hat{X}_{\mu\nu}\hat{X}^{\mu\nu} - \frac{\epsilon}{2}\hat{F}_{\mu\nu}\hat{X}^{\mu\nu} - \frac{1}{2}m_X\hat{X}^\mu\hat{X}_\mu, \quad (2.1)$$

where $\hat{F}_{\mu\nu}$ and $\hat{X}_{\mu\nu}$ are the field strength tensors corresponding to the SM photon field \hat{A}_μ and the dark photon \hat{X}_μ , respectively. The $U(1)$ kinetic mixing term in the Lagrangian effectively arises, at loop level, from the interaction between the \hat{X} boson and the $j_\mu^{L_\mu-L_\tau}$

current, as illustrated in Fig. 1. While in the general case the kinetic mixing parameter ϵ can be treated as a free parameter of the Lagrangian, in this specific construction it is given by [41]

$$\epsilon = \frac{eg_X}{2\pi^2} f(m_\mu, m_\tau, q), \quad (2.2)$$

with the loop factor

$$f(m_\mu, m_\tau, q) = \int_0^1 dx x(1-x) \ln \frac{m_\mu^2 - q^2 x(1-x)}{m_\tau^2 - q^2 x(1-x)}. \quad (2.3)$$

The explicit mass m_X of the DP may arise e.g. from higher scale interactions with an extended Higgs sector. In the following we will assume m_X in the few MeV to few GeV range. We do not consider additional explicit mass mixing with the much heavier Z -boson field, which is strongly constrained by electroweak precision measurements [68, 69]. Non-diagonal elements in the mass matrix inherited from the small kinetic mixing ϵ can also be safely neglected. With this choice, the mass eigenstates (\hat{A}, \hat{X}) are diagonal in the interaction basis (A, X) .

Theoretical consistency requires anomaly cancellation. Even after adding right-handed neutrinos fields, which allow for the observed neutrino oscillations, this minimal construction is automatically anomaly free. We give Dirac masses of $\mathcal{O}(1)$ eV to muon and tau neutrinos, but do not introduce Majorana masses, such that the mass eigenstates remain light.

The DP couples directly to muon and tau lepton flavours with coupling strength $\alpha_X = g_X^2/(4\pi)$, and to all electrically charged particles with effective coupling strength $\epsilon^2 \alpha_{\text{em}}$. It decays into all fermion anti-fermion pairs with fermion masses below $m_X/2$, with a partial decay width

$$\Gamma_i = \frac{1}{3} m_X (\delta_{i,(\mu,\tau)} \alpha_X + \epsilon^2 \alpha_{\text{em}} |q_i| N_c) \left(1 + \frac{2m_i^2}{m_X^2}\right) \sqrt{1 - \frac{4m_i^2}{m_X^2}} \theta(m_X - 2m_i), \quad (2.4)$$

where m_i and q_i denote the fermion's mass and charge respectively, and N_c is the number of colours (1 for leptons and 3 for quarks). The $\delta_{i,(\mu,\tau)}$ indicates that the tree-level contribution is present only for decays into muon and tau leptons. The DP decay into neutrino states (both left- and right-handed), neglecting their mass, also occurs at tree-level via its coupling to ν_μ and ν_τ flavours:

$$\Gamma_{\nu_i} = \frac{1}{3} m_X \delta_{\nu_i,(\nu_\mu,\nu_\tau)} \alpha_X. \quad (2.5)$$

The left panel of Fig. 2 shows the DP branching ratios as a function of its mass, clearly demonstrating the strong suppression of decay channels that proceed via kinetic mixing compared to those into fermions charged under $L_\mu - L_\tau$. The DP hadronic branching ratio is obtained by appropriately rescaling the experimental data for the ratio $R = \frac{\sigma(e^+e^- \rightarrow \text{hadr.})}{\sigma(e^+e^- \rightarrow \mu^+\mu^-)}$ [70]. Its contribution is small and irrelevant for our analysis, as the DP width is dominated by decays into muon and tau flavoured leptons above their mass threshold, and by decays into electrons below 500 MeV.

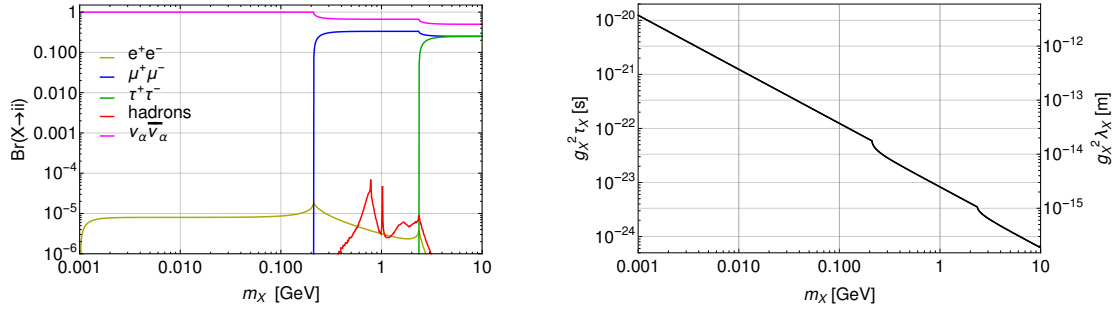


Figure 2. Branching ratio of DP as a function of its mass (left), and DP mean lifetime and decay length in the DP rest frame multiplied by g_X^2 as a function of its mass (right).

The mean lifetime τ_X and decay length λ_X of the DP in its rest frame are calculated as:

$$\tau_X = \frac{\lambda_X}{c} = \frac{\hbar}{\Gamma_X}, \quad \text{with} \quad \Gamma_X = \sum_s \Gamma_i \quad (2.6)$$

and are shown in the right panel of Fig. 2; in the plot we show the quantities $g_X^2 \tau_X$ and $g_X^2 \lambda_X$ which are independent of g_X .

3 Dark photon signatures at Belle II

Dark photons with masses between MeV and GeV are testable in low energy e^+e^- collisions. In the following, we focus on associated DP production at the Belle II experiment via the processes $e^+e^- \rightarrow XY$, where $Y = \gamma, f^+f^-$ and $f = e, \mu, \tau$ or hadrons. Belle II is a general purpose detector at the e^-e^+ collider KEKB which runs at the centre-of-mass energy $\sqrt{s} = 10.58$ GeV with an anti-symmetric beam energy setup ($E(e^-) = 7$ GeV, $E(e^+) = 4$ GeV). Operating mostly at the $Y(4S)$ resonance, its primary focus is to study B meson properties [71]. The Belle II detector covers an asymmetric phase space, with the polar angle spanning from $\theta_l = 5^\circ$ to $\theta_u = 150^\circ$, with the positive z -axis in the direction of the e^- beam. The Central Drift Chamber (CDC) has an inner tracker radius $R_T = 0.168$ m (with $R_T^2 = R_x^2 + R_y^2$) and barrel length $R_z = 1.15$ m. Its current data set corresponds to an integrated luminosity of $L = 427 \text{ fb}^{-1}$, while the ultimate target luminosity is $L = 50 \text{ ab}^{-1}$ [72].

In the following we discuss the relevant experimental signatures in the Belle II environment which are sensitive to DPs within the model introduced in Sect. 2. The final states considered comprise combinations of photons, leptons with prompt or displaced decay vertices, and of missing transverse energy/momentum originating from invisible DPs decays. Because of the DP's suppressed coupling to electrons, cf. Eq. (2.2), and the large SM background, we do not consider resonant processes with two body final states, $e^+e^- \rightarrow X \rightarrow f^+f^-$. Nevertheless, DPs can be produced through their unsuppressed couplings to muon and tau leptons, via the processes $e^+e^- \rightarrow \ell^+\ell^-X$ with $\ell = \mu, \tau$, i.e. when radiated off a heavy lepton final state. They can also be produced through kinetic mix-

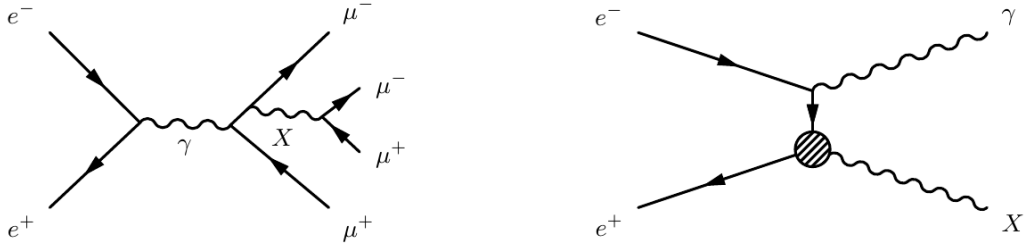


Figure 3. Feynman diagrams depicting the considered DP production processes at e^+e^- colliders. *Left:* Radiation off a muon or tau lepton. *Right:* Mono photon process.

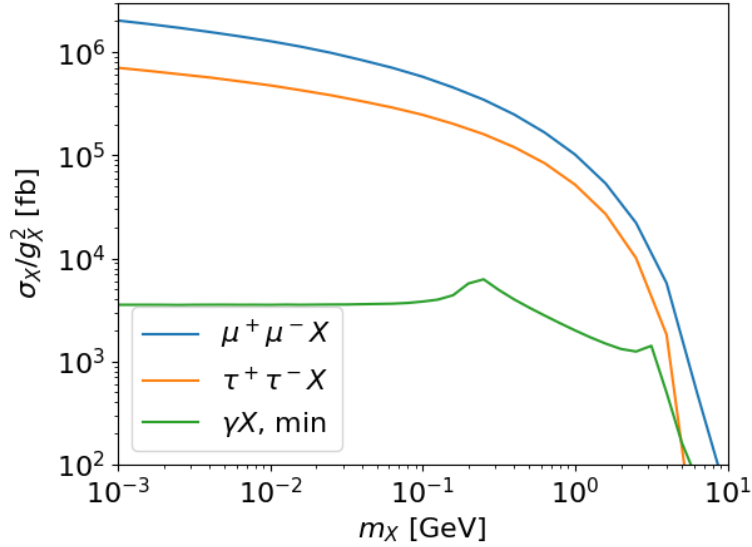


Figure 4. Dark photon production cross sections at Belle II (with $\sqrt{s} = 10.58$ GeV), divided by the $U(1)_{L_\mu-L_\tau}$ coupling constant, g_X^2 , for the production mechanisms in e^+e^- collisions as described in the text. The Belle II geometric detector acceptance has been imposed on the leptons and the photon, as well as a minimum energy cut of 1 GeV for the photon.

ing in association with a SM photon, via the one-loop induced process $e^+e^- \rightarrow \gamma X$, with amplitude proportional to ϵ^2 . The corresponding Feynman diagrams are shown in Fig. 3. Because of their very narrow width, we will exclusively consider DP on-shell production and set the momentum transfer to $q^2 = m_X^2$ when evaluating ϵ in Eq. (2.2). For example, in the regime where $m_X \ll m_\mu$, we obtain $\epsilon \simeq 0.015 g_X$, whereas $m_X = 10$ GeV yields $\epsilon \simeq 6 \times 10^{-4} g_X$. In Fig. 4 the cross sections, divided by the coupling constant, g_X^2 , for the three main production mechanisms, are shown as function of the DP mass in the Belle II detector acceptance region, including also a lower cut on the photon energy of 1 GeV.

The relevant processes for DP searches at Belle II are obtained combining the decay channels of the DP X , depicted in the left panel of Fig. 2, with the possible associated particles Y . Among the possible combinations, processes where both Y and the DP decay involve a combination of μ, τ, ν fermions are most relevant, due to their large production cross section and $\mathcal{O}(1)$ branching ratio. These signatures are expected to give the largest

$Y \backslash X \rightarrow$	ν	$e/\text{hadrons}$	μ/τ
ν	invisible	$r_W r_\epsilon$	r_W
$e/\gamma/\text{hadrons}$	r_ϵ	r_ϵ^2	r_ϵ
μ/τ	1	r_ϵ	1

Table 1. Four fermion final states from the process $e^+e^- \rightarrow XY$ as discussed in the text. Entries denote suppression factors due to the loop-induced coupling ϵ , or weak interactions. Leading processes are labelled “1”.

sensitivity to DP searches and could become “discovery channels”. In this group, we also include the so-called “monophoton” channel, where $Y = \gamma$ and the DP decays invisibly. This signature is somehow exceptional because, as we will discuss below, excellent background suppression can be achieved, and background free analyses are justified. For completeness we also consider the associated production of a DP with $Y = \nu\bar{\nu}$. This process occurs via weak interactions and is suppressed by a factor $r_W = s^2 G_f^2 \simeq 10^{-6}$ compared to QED processes with Fermi’s constant, $G_f = 1.166 \times 10^{-5} \text{ GeV}^2$ [70]. The cross sections for processes where $Y \neq \mu, \tau, \nu$ are loop-suppressed by a factor $r_\epsilon = \epsilon^2/g_X^2 < 10^{-4}$ compared to the discovery channels, and are therefore expected to provide lesser sensitivity. Final states stemming from DP decays into electrons or hadrons have branching ratios loop-suppressed by the same factor r_ϵ , therefore their cross sections are much smaller compared to the discovery channels. The discussed final states are summarised in Tab. 1, with their corresponding suppression factors with respect to the SM QED background.

Existing Belle II searches for light DPs mainly target final states with missing energy from the invisible decays of the DP. Analyses of the process $e^+e^- \rightarrow \mu^+\mu^-X$ with $X \rightarrow$ invisibles have been performed using a dataset corresponding to an integrated luminosity of 276 pb^{-1} [73] and, more recently, of 79.7 fb^{-1} [74], achieving exclusion limits between $g_X \simeq 3 \times 10^{-3}$ for DPs with $m_X \ll 1 \text{ GeV}$ and $g_X \simeq 1$ for DPs as heavy as 8 GeV . For the ultimate Belle II integrated luminosity goal of 50 ab^{-1} , an exclusion limit on the DP coupling down to $g_X \simeq \mathcal{O}(10^{-4})$ [73] is projected for this channel. Analyses targeting the specific $L_\mu - L_\tau$ gauge symmetry, exploiting alternative signatures, such as the monophoton channel with an assumed integrated luminosity of 20 fb^{-1} [75], and final states with DPs decaying into muon or tau pairs with an assumed integrated luminosity of 100 fb^{-1} [76], have demonstrated a promising sensitivity, comparable with the $2\mu + \cancel{E}$ final state.

Previous studies from the BaBar collaboration also reported searches for new light physics in final states with photons and leptons. They probed a general model with kinetic mixing between the SM photon and DPs, using the processes $e^+e^- \rightarrow \gamma\ell^+\ell^-$ with $\ell = e, \mu$, based on their complete dataset corresponding to a total luminosity of 514 fb^{-1} . Upper limits at 90% confidence level (CL) on ϵ were drawn between 10^{-4} and 10^{-3} for DP masses between 0.02 GeV and 10.2 GeV [22]. In the same mass range, a dedicated analysis on SM extensions with extra $U(1)'$ $L_\mu - L_\tau$ gauge symmetry, using the four muon final state [77], yielded the current, most stringent upper bound, $g_X = 7 \times 10^{-4}$.

	final state	σ_b
di-photon	$\gamma\gamma$	2.83 nb
radiative Bhabha scattering	$\gamma e^+ e^-$	63 nb
radiative neutrinos	$\gamma \bar{\nu} \nu$	3.64 fb
di-tau	$\tau^+ \tau^-$	0.8 nb
radiative di-muon	$\mu^+ \mu^- \gamma$	0.64 nb
di-electron di-muon	$e^+ e^- \mu^+ \mu^-$	14.9 nb
four muon	$2\mu^+ 2\mu^-$	189 fb
di-tau di-muon	$\tau^+ \tau^- \mu^+ \mu^-$	130 fb

Table 2. SM QED background processes for DP searches. Cross sections are computed for the fiducial volume of the Belle II detector, including the angular acceptance cut on the visible particles in the final states, and a minimum energy cut of 1 GeV for the photons.

4 Analysis setup

We have implemented the minimal DP model introduced in Sect. 2 into `Feynrules` [78] and generated the model file for the Monte Carlo event generator `WHIZARD` [79–81]. We then used `WHIZARD` to generate samples containing between 10^5 and 10^7 events, and to calculate cross sections for leading order signal and background processes. The complete information on the kinematics of each event is recorded in the four-vectors of the final state particles which are then used to compute the relevant observables for each of the analyses described in the following.

The finite resolution of the Belle II detector for particles’ momenta and energies is modelled by smearing the four-momenta following a normal distribution with standard deviations of 0.5% for muons and electrons, and of 5% for photon energies [82]. The energy resolution for charged particles is taken to be 5 MeV. Particle identification is highly important in order to study different event topologies at Belle II [83]. We consider the reconstruction efficiencies of photons as 100% for $E_A = \mathcal{O}(1)$ GeV, of muons $\sim 90\%$ and of electrons $\sim 95\%$ [25, 84]. Contributions from mis-reconstructed particles are neglected, since for muons they are as low as 0.9%, while the pion fake rate is 1.4% [85]. Complicated backgrounds such as decay chains of D mesons can also lead to the mis-identification of pions as muons or electrons, with a likelihood as high as 10% for pion momenta $P_\pi \leq 3$ GeV. This contribution is not included in our analyses, since we do not include QCD processes which are suppressed in this model.

The SM QED processes representing the background for DP searches and their fiducial cross sections are listed in Tab. 2. Most search channels are affected by enormous SM background rates which dominate the signatures for DP signals. In the following analyses we find optimised kinematic cuts to enhance the signal-over-background ratio. Specific observables are considered to discriminate the DP signals from the background. These are used to extract the experimental sensitivity on the model parameters at different luminosity stages. When background rates are much larger than the signal, $N_b \gg N_s$, the optimised combination of kinematic cuts for each phase space region is identified by minimising the

critical number of signal events for which the BSM hypothesis is excluded at a certain Confidence Level (CL):

$$N_s^{\text{crit}} = \frac{n (\sum_i \sigma_i \epsilon_i \times L)^{\frac{1}{2}}}{\epsilon_s}, \quad (4.1)$$

where the sum is over all contributing background processes with their respective cross sections σ_i and selection cut efficiencies ϵ_i . We choose $n = 2$ for a 95% one-sided CL, and ϵ_s is the overall selection cut efficiency for the signal. When the number of background events is less than $\mathcal{O}(100)$, we evaluate the critical number of signal events assuming a Poisson distribution, and calculate N_s^{crit} as

$$\sum_{k=0}^{N_b} \frac{\lambda^k e^{-\lambda}}{k!} = 1 - CL, \quad (4.2)$$

with $\lambda = N_s^{\text{crit}} + N_b$, and $CL = 95\%$. In the special case of a completely reducible background, i.e. in background free analyses, we obtain $N_s^{\text{crit}} = 2.99$. From N_s^{crit} we extract the critical signal cross section by $\sigma_s^{\text{crit}} = N_s^{\text{crit}}/(\epsilon_s L)$, from which in turn we obtain the critical value of g_X above which the signal is observable at the chosen confidence level.

5 Dark photon search channels

In the following we describe optimised analyses for each relevant search channel for DP detection at Belle II, i.e. for monophoton, two muon plus missing energy, four muon prompt, and four muon displaced signatures. In each channel, SM backgrounds partly arising because of the limited detector acceptance, will be discussed. To extract sensitivity contours in the model parameter space, the ultimate Belle II luminosity goal of 50 ab^{-1} is assumed, and DP masses are scanned in the range from 1 MeV to 10 GeV.

5.1 Monophoton

In this section we consider the monophoton signature consisting of a single observed photon together with missing transverse energy, i.e. $e^+e^- \rightarrow \gamma + \cancel{E}$, see e.g. Ref. [75]. The DP contributes to this signature as \cancel{E} when it decays into an invisible final state or outside of the detector acceptance. The dominant contribution to this signature stems from the decays into μ and τ neutrinos, $X \rightarrow \nu_\alpha \bar{\nu}_\alpha$, with $\alpha = \mu, \tau$, which have a large $\mathcal{O}(1)$ branching ratio, while the fraction of decays outside the detector phase space contributes always below one percent to the total DP signal and can thus be neglected.

The most relevant SM background processes contributing to the monophoton signature are: di-photon processes ($e^+e^- \rightarrow \gamma\gamma$) where one photon escapes detection; radiative Bhabha scattering ($e^+e^- \rightarrow \gamma e^+e^-$) where the final state leptons are undetected; and processes with a photon and one off-shell Z -boson decaying invisibly ($e^+e^- \rightarrow Z\gamma$ with $Z \rightarrow \nu\bar{\nu}$). The inclusive cross sections of these SM processes are given in Tab. 2, taking into account the geometric acceptance of the detector and including a photon energy lower cut of 1 GeV to suppress various backgrounds [75, 86]. The large di-photon and radiative Bhabha production cross sections also lead to a large number of monophoton events due

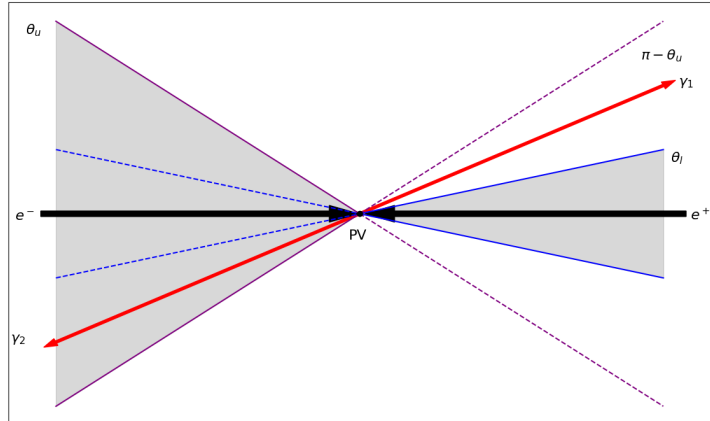


Figure 5. Schematic picture in the lab frame of a monophoton background event arising from the di-photon process $e^+e^- \rightarrow \gamma\gamma$ due to the detector geometry.

to the gap in acceptance coverage between the forward and backward hemispheres of the Belle II detector. Monophoton signatures from these final states occur when one photon, or the lepton pair, is missed. Such a scenario is depicted in Fig. 5, where one photon, γ_1 , is in the forward direction with an angle larger than $\theta_l = 5^\circ$, while the second photon, γ_2 , escapes detection in the backward direction with an angle larger than $\theta_u = 150^\circ$. The background contribution from the electro-weak process with a Z -boson decaying into neutrinos was not considered in previous analyses [75] because of its comparatively small cross section. Nevertheless, we expect a significant contribution from this SM background process because of the high target luminosity of the Belle II experiment, and we therefore include this contribution in our analysis.

We simulate event samples at tree-level containing 10^6 events for the DP signal in the mass range $10 \text{ MeV} \leq m_X \leq 10 \text{ GeV}$, 10^6 events for the SM di-photon and off-shell Z into neutrinos processes, and 10^5 events for the radiative Bhabha process. Di-photon and radiative Bhabha samples are produced with no angular acceptance cuts on the final state particles. We extract contributions to the monophoton SM background from these two processes, selecting the events where respectively one of the photons or the electron-positron pair are outside of the detector acceptance. To the di-photon sample, we apply the following selection condition:

$$(\theta_l < \theta_{\gamma_i} < \theta_u) \quad \text{and} \quad (\theta_{\gamma_j} < \theta_l \text{ or } \theta_{\gamma_j} > \theta_u), \quad \text{with} \quad i \neq j \quad \text{and} \quad i, j = 1, 2, \quad (5.1)$$

where θ_{γ_i} is the angle of photon γ_i with respect to the positive beam axis, and $\theta_l = 5^\circ$ and $\theta_u = 150^\circ$. The surviving monophoton events amount to about 20% of the original di-photon sample. They populate a characteristic phase space region, with the photon being quite energetic $E_\gamma \gtrsim 5.5 \text{ GeV}$ and in a narrow forward region $\theta_l < \theta_\gamma < \pi - \theta_u$. Similarly, from the radiative Bhabha sample, we select monophoton events when electron and positron both have angles bigger than θ_u . This selection cut is very effective and

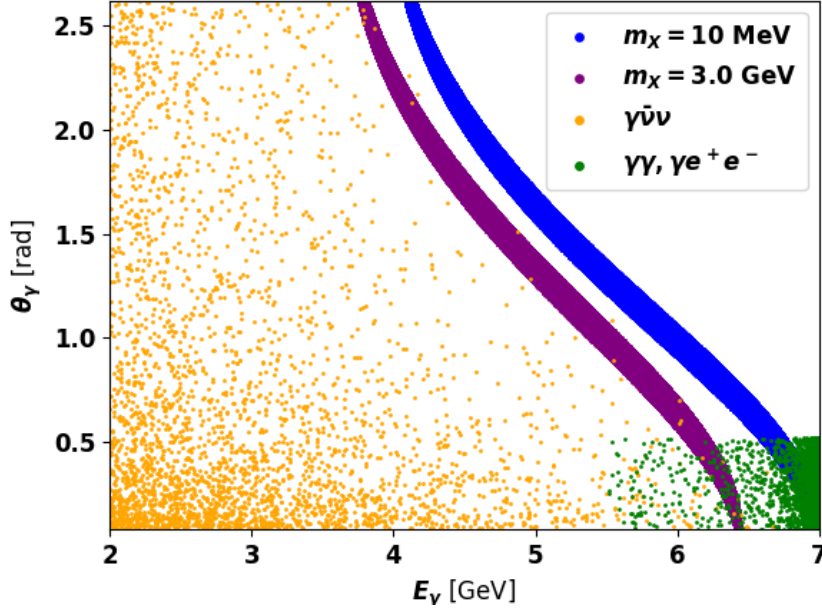


Figure 6. Distribution in angle and energy of the monophoton events from DP signals with $m_X = 10$ MeV and $m_X = 3.0$ GeV (blue and purple respectively), from SM QED di-photon and radiative Bhabha processes (green), and for the irreducible EW Z to neutrinos process (yellow). The displayed parameter space reflects the detector’s angular acceptance of the photon.

reduces the sample by a factor of 10^{-4} , confining the photon to the same phase space region as the di-photon sample. In Fig. 6 we show the distribution in angle and energy for the three SM background processes, and for two representative signals with $m_X = 10$ MeV and $m_X = 3.0$ GeV.

In the DP signal samples, the photon’s angle and energy are tightly correlated and all the signal events are bound to a narrow band in the θ_γ - E_γ plane. The background events from di-photon and radiative Bhabha samples populate a defined phase space region, and can be entirely removed with a simple selection cut $\theta_\gamma > 20^\circ$, which has selection efficiencies on the signal $\epsilon_S = 0.62 - 0.68$, across the DP mass range and on the processes with a photon and one off-shell Z -boson $\epsilon_{\gamma\nu\bar{\nu}} = 0.58$. The off-shell Z -boson sample constitutes an irreducible background for the DP signal in this channel, as its topology is identical to the DP signal, despite the Z -boson being much heavier than the DP in this model. The heavy Z -boson takes most of the energy of the process and the photon is preferentially soft, and we observe no clear correlation between its angle and energy.

Exploiting these kinematic features of signal and background, for each DP mass choice we define an optimal search region which maximises our sensitivity to the DP signal. For this, we consider bins of width $\Delta E = 0.35$ GeV for photon energies between 2 GeV and 7 GeV, compatible with the detector energy resolution of 5% for $E \sim 7$ GeV [71]. For each energy bin we identify an interval in the angle θ_γ which encloses all DP signal events in the particular bin. In each phase space area we evaluate the remaining number of

m_X [MeV]	$E_{\mu\mu}$ [GeV]	θ_X [rad]	$\epsilon_{\gamma\nu\bar{\nu}}$ (%)	ϵ_X (%)	σ_X^{crit} [fb]
1	[4.08, 6.88]	[0.33, 2.62]	0.138	62.1	12.99
2	[4.08, 6.88]	[0.33, 2.62]	0.1381	62.1	13.0
3	[4.08, 6.88]	[0.33, 2.62]	0.1381	62.1	13.0
4	[4.08, 6.88]	[0.33, 2.62]	0.1379	62.0	12.99
5	[4.08, 6.88]	[0.33, 2.62]	0.1378	62.0	12.98
6	[4.08, 6.88]	[0.33, 2.62]	0.1379	62.1	12.99
7	[4.08, 6.88]	[0.33, 2.61]	0.1379	62.0	12.99
8	[4.08, 6.88]	[0.33, 2.62]	0.1380	62.0	12.99
9	[4.08, 6.88]	[0.33, 2.62]	0.1380	62.0	12.99
10	[4.08, 6.88]	[0.33, 2.62]	0.1379	62.1	12.99
20	[4.08, 6.88]	[0.33, 2.62]	0.1381	62.1	13.0
30	[4.08, 6.88]	[0.33, 2.62]	0.1379	62.0	12.99
40	[4.08, 6.88]	[0.33, 2.62]	0.1379	62.0	12.99
50	[4.08, 6.88]	[0.33, 2.62]	0.1381	62.0	13.0
60	[4.08, 6.88]	[0.33, 2.62]	0.1381	62.0	13.0
70	[4.08, 6.88]	[0.33, 2.62]	0.1381	62.0	13.0
80	[4.08, 6.88]	[0.33, 2.62]	0.1383	62.0	13.01
90	[4.08, 6.88]	[0.33, 2.62]	0.1383	62.0	13.02
100	[4.08, 6.88]	[0.33, 2.62]	0.1383	62.1	13.02
200	[4.08, 6.88]	[0.33, 2.62]	0.1395	62.1	13.10
300	[4.08, 6.88]	[0.33, 2.62]	0.1420	62.1	13.28
400	[4.08, 6.88]	[0.33, 2.62]	0.1451	62.2	13.51
500	[4.07, 6.87]	[0.33, 2.62]	0.1494	62.2	13.82
600	[4.07, 6.87]	[0.33, 2.62]	0.1533	62.2	14.10
700	[4.06, 6.86]	[0.33, 2.62]	0.1588	62.2	14.50
800	[4.06, 6.86]	[0.33, 2.62]	0.1653	62.3	14.97
900	[4.05, 6.85]	[0.33, 2.62]	0.1734	62.3	15.56
1000	[4.05, 6.85]	[0.33, 2.62]	0.1826	62.3	16.22
2000	[3.94, 6.39]	[0.33, 2.62]	0.3791	62.8	23.66
3000	[3.75, 6.20]	[0.33, 2.62]	0.8536	63.6	34.88
4000	[3.50, 5.60]	[0.33, 2.62]	1.5951	64.4	47.10
5000	[3.17, 5.27]	[0.33, 2.62]	3.1284	65.4	65.34
6000	[2.77, 4.52]	[0.33, 2.62]	5.3237	66.7	84.75
7000	[2.30, 3.70]	[0.33, 2.62]	9.4203	67.6	112.22
8000	[2.00, 2.70]	[0.33, 1.98]	11.3389	59.7	122.96

Table 3. Selection cuts in the monophoton channel for the considered DP masses for the two observables: DP energy, E_X and angle w.r.t the beam axis θ_X . Column $\epsilon_{\gamma\nu\bar{\nu}}$ denotes the selection efficiency for the SM background $\nu\bar{\nu}$ final state, which already includes the efficiency of the $\theta_\gamma > 20^\circ$ cut. Column ϵ_X contains the selection efficiency on the signal, and the last column, σ_X^{crit} , shows the critical cross section above which the signal is visible at 95% CL.

background events from the SM process $\gamma\bar{\nu}\nu$, finding a suppression of $\mathcal{O}(10^{-5})$ for all m_X considered. The sensitivity of Belle II to DP parameters is evaluated according to Sect. 4, using $\epsilon_\gamma = 0.99$ for the reconstruction efficiency of a photon with energy at or above 2 GeV [87]. The resulting sensitivity contour, for an integrated luminosity of 50 ab^{-1} , is displayed in Fig. 11 (dotted dark blue line) and discussed in Sect. 6.

5.2 Two muons plus missing energy

We now discuss the signature of two muons with missing transverse energy, $e^+e^- \rightarrow \mu^+\mu^- + \cancel{E}$. The signal in this channel originates from a DP, radiated from a muon and then decaying invisibly into muon or tau neutrinos: $e^+e^- \rightarrow \mu^+\mu^- + X \rightarrow \mu^+\mu^- \nu_{\mu,\tau} \bar{\nu}_{\mu,\tau}$. The contribution from DPs decaying outside the detector acceptance is at most at the sub-percent level for most of the considered parameter space, and will therefore be neglected. Two SM background processes contribute to this signature with sizeable event rates and constitute irreducible backgrounds for the analysis. The first arises from di-tau production where both taus decay into muons, $e^+e^- \rightarrow \tau^+\tau^-$ and $\tau^\pm \rightarrow \mu^\pm \nu_\mu \bar{\nu}_\tau$, with cross section $\sigma_{\tau\tau \rightarrow \mu\mu} = 0.8 \text{ nb} \times \text{Br}(\tau \rightarrow \mu)^2 \times \epsilon_{\mu\mu}$, where $\text{Br}(\tau \rightarrow \mu) = 17.39\%$ is the branching ratio of the tau lepton into muons. An efficiency of $\epsilon_{\mu\mu} = 0.78$ for this background, due to the geometric acceptance for the two muons, has been determined from simulation. The second SM background is di-muon production with a hard photon radiated outside the detector acceptance region, $e^+e^- \rightarrow \mu^+\mu^- \gamma_{\text{inv}}$, with the cross section estimated to be $\sigma_{\mu\mu\gamma} = 0.64 \text{ nb}$ (see. Tab. 2).

We simulate 10^6 events for the signal and each background process. The following observables are constructed from the muons' four-momenta: di-muon energy $E_{\mu\mu}$, three momentum $P_{\mu\mu}$, and angle $\theta_{\mu\mu}$ with respect to the electron beam direction, and the di-muon opening angle $\alpha_{\mu\mu}$. In addition we also construct the recoil mass of the di-muons, which is defined as

$$m_{\text{recoil}}^2 = (E_{e^-} - E_{\mu\mu})^2 - \Delta E^2 - P_{\mu\mu}^2 + 2\Delta E \cos(\theta_{\mu\mu})P_{\mu\mu}, \quad (5.2)$$

where $E_{e^-} = 11 \text{ GeV}$ is the electron beam energy, and $\Delta E = 3 \text{ GeV}$ is the difference between electron and positron beam energies. The recoil mass peaks at m_X^2 for the DP signal, at zero for the radiative di-muon background, and it is smeared from 0 to s for the di-tau background due to the energy carried away by the neutrinos from the tau decays. Optimal cuts in the observables $\alpha_{\mu\mu}$, $\theta_{\mu\mu}$ and $P_{\mu\mu}$ were found to improve the sensitivity only marginally, and will hence not be discussed in the following. We study the distributions of the observables for the signal with $10 \text{ MeV} \leq m_X \leq 7 \text{ GeV}$, and for the SM backgrounds. Optimal cuts for each DP mass are found by minimising the number of background events to obtain a visible signal at 95% CL according to Eq. (4.1). We find that the two most relevant observables for signal-over-background enhancement are the recoil mass m_{recoil}^2 and $E_{\mu\mu}$, whose distributions are shown in Fig. 7 for DP masses of $m_X = 10, 100, 1000, 3000 \text{ MeV}$ and $g_X = 0.001$. Given the shape of the recoil mass distribution, we find that appropriate cuts in this observable can almost completely remove contributions from the di-muon background for $m_X \geq 1 \text{ GeV}$, in agreement with the results

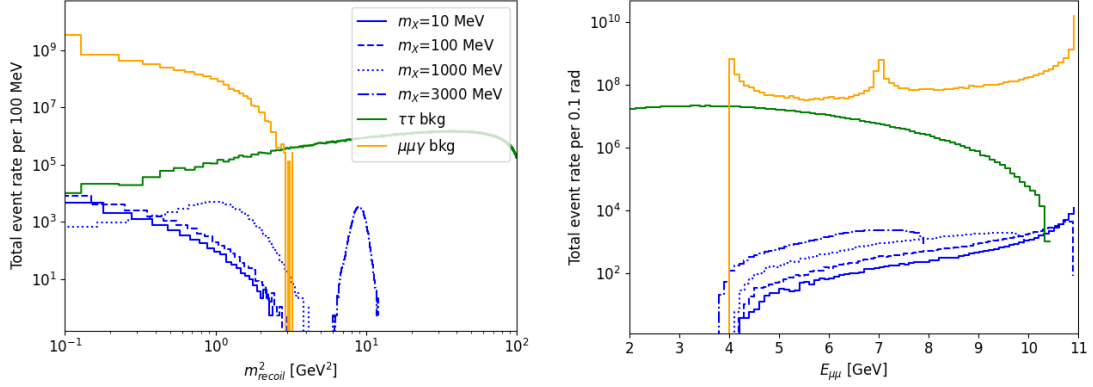


Figure 7. Event rates as function of the recoil mass m_{recoil}^2 (left) and of the di-muon energy $E_{\mu\mu}$ (right), normalised as indicated in the axes captions. The blue signal curves correspond to the choices $m_X = 10, 100, 1000$ and 3000 MeV and $g_X = 0.001$. The green curves denote the di-tau background and include the decay $\text{Br}(\tau \rightarrow \mu)$. The yellow curves denote the radiative di-muon background for this signature.

of Ref. [75]. For DPs with $m_X \geq 1$ GeV, the most effective way to disentangle the signal from the background is through optimal cuts in the $E_{\mu\mu}$ observable. In Tab. 4 we list the considered DP masses, the selection cuts for each search regions, their efficiencies for signal and the two SM backgrounds. The critical signal cross sections in the last column are obtained assuming an integrated luminosity of 50 ab^{-1} , and they translate in the 95% CL exclusion solid dark blue contour line in Fig. 11.

5.3 Four muons prompt

We study the sensitivity of the Belle II experiment on the DP signal in the final state with two muon pairs, $e^+e^- \rightarrow \mu^+\mu^+\mu^-\mu^-$, which we will refer to as the 4μ channel in the following. The DP signal in this channel stems from a DP radiated from a muon and decaying into a muon pair, see the left panel of Fig. 3. The main SM background is from the QED process with two photons decaying into muon pairs and has a cross section of $\sigma_{4\mu} = 189 \text{ fb}$. Here we neglect additional possible backgrounds with hadronic final states where pions are misidentified as muons, which has a probability of 1.4% per pion only.

We simulate 10^6 events within the geometric acceptance for the background, and 10^6 signal events in each of the suitably chosen bins in the mass range $220 \text{ MeV} \leq m_X \leq 8 \text{ GeV}$, see Tab. 5 for details. In the signal samples, the DP propagator is taken to be on-shell as the DP is very narrow. The DP kinematics is then reconstructed by identifying the muon pair with an invariant mass $m_X \pm 5 \text{ MeV}$, thus taking into account the finite detector resolution. With this procedure, the signal selection efficiency is basically 100% in all bins. Due to the tight selection, the resulting background suppression ranges from around 2% in bins with m_X close to the di-muon threshold, to $\sim 0.2\%$ for $m_X \simeq \sqrt{s}$. This is visible in Fig. 8 where the number of background events within each search window is shown.

To achieve the best sensitivity for DP signals in this channel, we consider four observables for the DP candidates: energy E_X , momentum, angle θ_X with respect to the beam axis, and opening angle of the two additional muons. The distributions for E_X and θ_X

m_X [MeV]	m_{recoil}^2 [GeV ²]	$E_{\mu\mu}$ [GeV]	$\epsilon_{\mu\mu\gamma}(\%)$	$\epsilon_{\tau\tau}(\%)$	$\epsilon_X(\%)$	σ_X^{crit} [fb]
1	[-4.2, 3.1]	[7.2, 11]	16.1	0.56	29.3	8.82
2	[-4.4, 3.3]	[5.5, 11]	54.1	0.69	99.6	4.75
3	[-3.7, 3.2]	[5.5, 11]	51.3	0.63	99.6	4.63
4	[-4.2, 3.3]	[5.2, 11]	49.7	0.67	99.7	4.55
5	[-4.3, 3.6]	[5.2, 11]	20.6	0.83	42.2	6.93
6	[-4.0, 3.6]	[5.2, 11]	20.6	0.80	43.9	6.66
7	[-4.5, 3.3]	[5.2, 11]	46.0	0.69	99.7	4.38
8	[-4.2, 3.4]	[5.2, 11]	20.6	0.72	46.7	6.26
9	[-4.4, 3.7]	[5.2, 11]	44.4	0.87	99.7	4.30
10	[-4.4, 3.4]	[5.2, 11]	43.7	0.73	99.7	4.27
20	[-4.4, 3.8]	[4.8, 11]	39.4	0.92	99.8	4.05
30	[-4.3, 3.7]	[4.8, 11]	36.8	0.84	99.8	3.92
40	[-4.6, 3.8]	[4.8, 11]	34.9	0.90	99.8	3.81
50	[-4.2, 3.5]	[4.8, 11]	33.6	0.77	99.8	3.74
60	[-5.6, 3.8]	[4.8, 11]	20.1	0.93	69.3	4.17
70	[-5.2, 3.6]	[4.8, 11]	20.0	0.83	70.8	4.07
80	[-5.0,-0.1]	[7.5, 11]	4.9	0.003	23.8	5.98
90	[-4.8, 3.9]	[4.8, 11]	19.7	0.96	73.6	3.88
100	[-4.4,-0.1]	[7.5, 11]	5.5	0.003	27.2	5.55
200	[-4.3,-0.3]	[7.4, 11]	3.1	0.001	18.9	6.00
300	[0.08, 4.1]	[7.4, 11]	5.1	0.85	39.6	3.68
400	[0.05, 4.2]	[7.4, 11]	5.7	0.89	48.8	3.14
500	[0.38, 4.6]	[7.9, 10]	1.3	0.91	23.5	3.18
600	[0.26, 4.5]	[7.6, 10]	2.4	0.98	43.1	2.35
700	[0.43, 4.7]	[7.8, 10]	1.3	0.98	37.3	1.96
800	[0.10, 5.0]	[5.3, 10]	6.0	1.45	75.5	2.10
900	[0.10, 5.1]	[5.0,9.8]	5.5	1.48	72.9	2.08
1000	[0.25, 5.5]	[7.3, 10]	2.5	1.38	65.1	1.59
2000	[2.1, 8.3]	[6.7,9.0]	0.1	2.65	71.6	0.349
3000	[5.9, 13]	[3.8,8.0]	0.0	5.81	99.8	0.307
4000	[13, 20]	[3.5,7.0]	0.0	7.33	99.7	0.345
5000	[22, 28]	[3.2,6.0]	0.0	7.85	99.7	0.357
6000	[34, 39]	[2.8,5.0]	0.0	7.61	99.6	0.352
7000	[47, 52]	[2.3,3.9]	0.0	6.29	92.2	0.346
8000	[62, 67]	[1.8,2.9]	0.0	4.51	86.7	0.312
9000	[80, 83]	[1.9,1.9]	0.0	0.05	21.6	0.135

Table 4. Selection cuts in the di-muon plus missing energy channel for the considered DP masses for the two observables: recoil mass m_{recoil}^2 and di-muon energy $E_{\mu\mu}$. Columns labelled $\epsilon_{\mu\mu\gamma}$ and $\epsilon_{\tau\tau}$ denote the selection efficiency for the SM background processes with $\mu\mu\gamma$ and $\tau\tau$ final states respectively. Column ϵ_X contains the selection efficiency on the signal, and the last column, σ_X^{crit} , shows the critical cross section above which the signal is visible at 95% CL.

m_X [MeV]	$m_{\mu\mu}$ [GeV]	$\epsilon_{m_{\mu\mu}}$ (%)	E_X [GeV]	θ_X [rad]	$\epsilon_{4\mu}$ (%)	ϵ_X (%)	σ_X^{crit} [fb]
220	[0.215, 0.225]	1.5	[0.220, 3.888]	[9.6e-05, 3.1]	1.0	90.3	0.013
230	[0.225, 0.235]	2.0	[0.230, 3.884]	[0.00026, 3.0]	1.3	90.1	0.015
240	[0.235, 0.245]	2.2	[0.240, 3.892]	[0.00011, 3.1]	1.4	90.0	0.016
250	[0.245, 0.255]	2.3	[0.250, 3.900]	[0.00034, 3.1]	1.5	89.8	0.017
260	[0.255, 0.265]	2.3	[0.260, 3.895]	[0.00026, 3.1]	1.4	89.6	0.017
270	[0.265, 0.275]	2.3	[0.270, 3.902]	[0.00029, 3.0]	1.5	89.5	0.017
280	[0.275, 0.285]	2.3	[0.280, 3.910]	[0.00035, 3.1]	1.4	89.5	0.016
290	[0.285, 0.295]	2.3	[0.290, 3.922]	[0.00066, 3.0]	1.4	89.4	0.016
300	[0.295, 0.305]	2.2	[0.300, 3.923]	[0.00021, 3.0]	1.4	89.2	0.016
350	[0.345, 0.355]	1.9	[0.350, 3.937]	[0.0013, 3.1]	1.2	88.6	0.015
400	[0.395, 0.405]	1.7	[0.400, 3.968]	[0.00017, 3.0]	1.0	88.2	0.014
450	[0.445, 0.455]	1.5	[0.450, 3.984]	[0.0019, 3.1]	0.8	87.8	0.013
500	[0.495, 0.505]	1.3	[0.500, 3.699]	[0.0024, 3.1]	0.7	83.7	0.012
550	[0.545, 0.555]	1.2	[0.550, 3.719]	[0.17, 3.1]	0.6	83.1	0.011
600	[0.595, 0.605]	1.1	[0.600, 3.746]	[0.17, 3.1]	0.5	82.8	0.011
650	[0.645, 0.655]	1.0	[0.650, 3.780]	[0.022, 3.1]	0.5	82.5	0.010
700	[0.695, 0.705]	1.0	[0.700, 3.802]	[0.17, 3.0]	0.4	82.1	0.010
750	[0.745, 0.755]	0.9	[0.750, 3.520]	[0.33, 3.1]	0.3	76.9	0.009
800	[0.795, 0.805]	0.9	[0.800, 3.860]	[0.13, 3.1]	0.4	81.7	0.009
850	[0.845, 0.855]	0.8	[0.850, 3.577]	[0.47, 3.1]	0.3	76.2	0.009
900	[0.895, 0.905]	0.8	[0.900, 3.608]	[0.49, 3.1]	0.3	75.9	0.008
950	[0.945, 0.955]	0.8	[0.950, 3.636]	[0.52, 3.1]	0.3	75.6	0.008
1000	[0.995, 1.005]	0.8	[1.000, 3.671]	[0.54, 3.0]	0.3	75.5	0.008
2000	[1.995, 2.005]	0.6	[2.000, 4.017]	[1.0, 3.1]	0.2	65.8	0.007
3000	[2.995, 3.005]	0.5	[3.000, 4.481]	[1.5, 3.1]	0.1	57.7	0.007
4000	[3.995, 4.005]	0.4	[4.000, 6.438]	[1.3, 3.1]	0.3	92.8	0.007
5000	[4.995, 5.005]	0.3	[5.000, 7.115]	[1.6, 3.1]	0.3	94.9	0.007
6000	[5.995, 6.005]	0.2	[6.000, 7.778]	[1.8, 3.1]	0.2	96.2	0.006
7000	[6.995, 7.005]	0.2	[7.000, 8.358]	[2.0, 3.1]	0.2	94.2	0.006
8000	[7.995, 8.005]	0.2	[8.000, 9.184]	[2.1, 3.1]	0.2	98.4	0.005
9000	[8.995, 9.005]	0.2	[9.065, 9.844]	[2.3, 3.1]	0.2	99.5	0.005

Table 5. Selection cuts for the 4μ channel for the considered DP masses. Column $m_{\mu\mu}$ contains the invariant mass selection cuts, and $\epsilon_{m_{\mu\mu}}$ the corresponding fraction of background events in that interval. Columns E_X and θ_X give the selection cuts on the two observables. Columns $\epsilon_{4\mu}$ and ϵ_X contain the efficiency of the combined cuts on the background and signal respectively. The last column, σ_X^{crit} , shows the critical cross section above which the signal is visible at 95% CL.

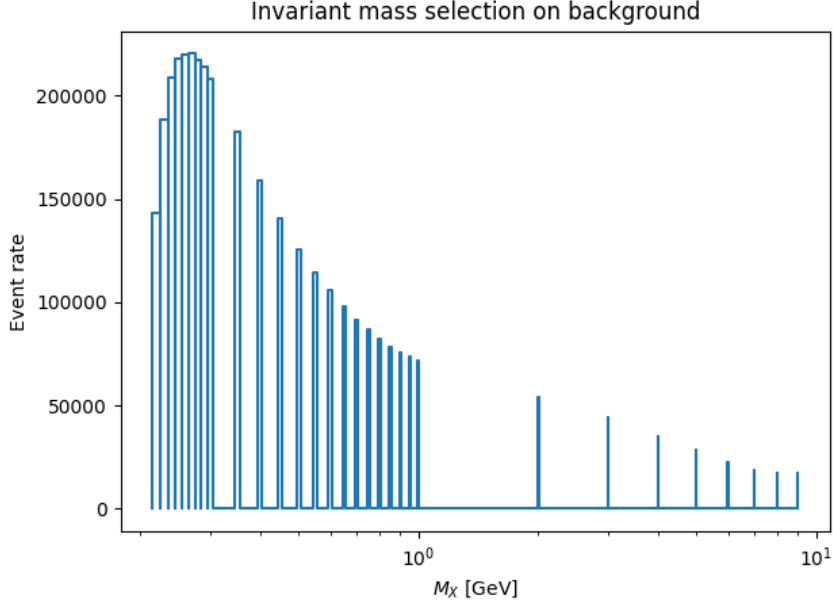


Figure 8. Distribution of 10^7 background events using the bin scheme as defined in Table 5. The events in each bin represent the background for each DP mass search region.

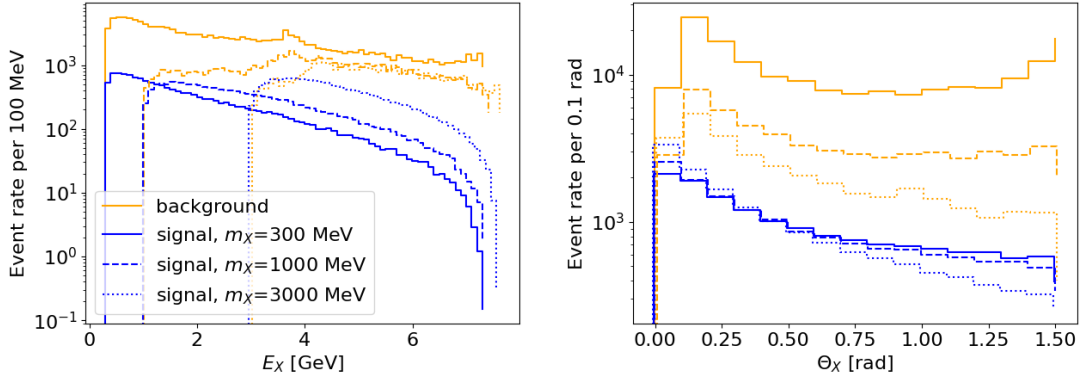


Figure 9. Energy and angular distributions of dark photon signals (blue) and SM background (yellow) in the 4μ final state at Belle II with integrated luminosity of 50 ab^{-1} . Signal curves are shown for $m_X = 300, 1000$ and 3000 MeV .

are shown in Fig. 9 for the background and for signals from DP masses $m_X = 300, 1000$ and 3000 MeV . For each DP mass used in the scan, optimal cuts on the four kinematic observables are determined to maximise the 95% CL signal exclusion, following Eq. (4.1). We find that cuts on E_X and θ_X lead to the best signal over background enhancement. A list of the optimised cuts for some representative DP masses is given in Tab. 5, together with the corresponding signal and background efficiencies due to the optimised cuts but after the initial invariant mass selection.¹ The last column gives the critical signal cross sections for an integrated luminosity of 50 ab^{-1} , from which we obtain the 95% CL exclu-

¹Note that because of the Gaussian smearing θ_X can assume values smaller than zero.

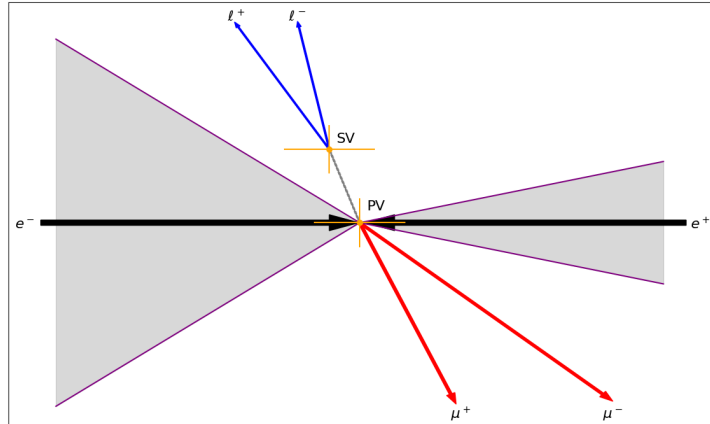


Figure 10. Schematic description of the process $e^+e^- \rightarrow \mu^+\mu^-X$, where X propagates a macroscopic distance and decays into $\ell^+\ell^-$. The primary vertex is denoted by ‘PV’ and is identified with the intersection of the two muon tracks (red arrows), the secondary vertex is denoted with ‘SV’ and identified with the intersection of the two lepton tracks (blue arrows). Uncertainties in the PV and SV positions are indicated by the yellow error bars. The electron and positron beams are denoted by black arrows, the detector acceptance is indicated by the purple lines, where the grey regions are invisible.

sion dashed-dotted dark blue contour line in Fig. 11, following the procedure described in Sect. 4.

5.4 Displaced vertices

We consider a special signature in the 4ℓ final state which features two interaction vertices separated by a measurable distance. The position of the decay vertices is reconstructed from the information collected in the Vertex detector (VXD), which is the closest sub-detector to the interaction point [88], and whose main purpose is to study the decay of tau leptons and B and D mesons. The design and the performance of the VXD [89, 90] allow a displacement resolution in the transverse plane as precise as a few micrometers [91]. A displaced signature is observed when the distance between the two vertices exceeds the detector resolution. This is schematically depicted in Fig. 10, where the Primary Vertex (PV) is on the nominal beam axis while the Secondary Vertex (SV) is displaced.² In our analysis for displaced vertices, we consider spatial detector resolutions of 5 and $10\text{--}\mu\text{m}$, which is somewhat optimistic compared to the recent study [92], but potentially achievable in the future as dedicated studies on the VXD performances are ongoing [93].

In the $L_\mu - L_\tau$ model considered here, a light DP with mass ~ 200 MeV and gauge coupling $g_X \sim 10^{-3}$ has a decay length in its rest frame $\lambda_X \sim 0.02 \mu\text{m}$ (see Fig. 2). The

²The position of the vertices along the beam direction is reconstructed less precise than that in the transverse plane. For our analysis, we will therefore only make use of the transverse displacement. We have checked that including information in the longitudinal displacement, even under optimistic assumptions, adds only marginally to the derived sensitivities.

additional boost into the Belle II laboratory frame can enhance the DP decay length up to a factor 10. Therefore, with the assumed vertex resolution and the high integrated luminosity collected at Belle II, a statistically significant number of DP decays, which populate the tail of the decay distributions, will appear as events with a displaced vertex. In principle, DP decays into any charged lepton contribute, but decays into electrons are strongly suppressed by the factor ϵ^2 (cf. Eq. (2.2)) compared to muons, whereas decays into taus require $m_X > 2m_\tau \simeq 3.5$ GeV, where the DP lifetime is small. We will therefore focus on displaced signatures with four muons.

SM background contributions with displaced final states include intermediate particles with a finite life-time such as B mesons and τ leptons. However, the Belle II detector is designed to perform precision measurements on the former, which have a very different topology compared to the DP signals considered, since on average B decays yield many tracks and include several mesons. Since the likelihood to misidentify several pions (or kaons) as muons is tiny, we assume that this background is sufficiently suppressed by the requirement of a four muon final state. The SM process $e^+e^- \rightarrow \tau^+\tau^-\mu^+\mu^-$ with $\tau^\pm \rightarrow \mu^\pm \bar{\nu}_\mu \nu_\tau$ has a cross section of about 4 fb and can feature displaced vertices because of the finite decay length of the relativistic τ lepton $\lambda_\tau \simeq 10^{-4}$ m. This background can be vetoed by requiring the total deposited energy to be within 3% of \sqrt{s} , reducing the predicted number of such events to 0.1 for 50 ab^{-1} . The only relevant background for our analysis originates from the SM QED process with four muons in the final state where, because of the finite detector resolution, a virtual photon decay may appear with a visible displacement.

We generate 10^7 background events, and 10^6 signal events for the DP masses in the restricted range $m_X = [220, 400]$ MeV, as detailed in Tab. 6. Because heavy DPs have an average shorter decay length, in our model we lose sensitivity at higher masses, where the decay length is too short for the determination of the displaced vertex. The background analysis in the displaced signature case closely follows the procedure defined for the prompt channel, starting with the reconstruction of the muon pair with an invariant mass $m_X \pm 5$ MeV. The fraction of background events within each search region is identical to the prompt analysis, and their distribution is shown in Fig. 8.

In the simulation of background and signal samples, random displacements are assigned to each muon track origin, accounting for both the finite detector resolution and finite life-time of the DP. The effect of the finite detector resolution is simulated by drawing all displacements from a normal distribution with standard deviation equal to the considered detector resolution. For this, the track origins projected on the transverse x - y plane are obtained by multiplying the random Gaussian shifts by $p_i/|\mathbf{p}|$, with $i = x, y$.³ This factor has been chosen to model the information on the position of the origin of the muons, which is derived from the particles' reconstructed tracks and momenta according to their energy deposition in the ECAL layers. Effectively, with this procedure, the origin of each muon track lays in the direction of the particle momentum. In the signal samples, an additional

³We chose to rescale the displacement according to the total momentum, rather than the transverse momentum, in order to account for the boost component along the beam axis.

m_X [MeV]	$m_{\mu\mu}$ [GeV]	$\epsilon_{m_{\mu\mu}}$ (%)	BFD [μm]	ϵ_X (%)	Max N_{sig}
220	[0.215, 0.225]	1.5	13.86	0.36	5.770
230	[0.225, 0.235]	2.0	14.45	0.28	5.907
240	[0.235, 0.245]	2.2	13.90	0.27	6.125
250	[0.245, 0.255]	2.3	14.62	0.23	5.357
260	[0.255, 0.265]	2.3	15.08	0.19	4.597
270	[0.265, 0.275]	2.3	14.15	0.20	4.865
280	[0.275, 0.285]	2.3	13.42	0.21	4.966
290	[0.285, 0.295]	2.3	13.96	0.18	4.142
300	[0.295, 0.305]	2.2	14.14	0.17	3.767
310	[0.305, 0.315]	2.2	13.86	0.16	3.662
320	[0.315, 0.325]	2.1	13.50	0.16	3.544
330	[0.325, 0.335]	2.1	13.98	0.14	3.120
340	[0.335, 0.345]	2.0	13.05	0.15	3.225
350	[0.345, 0.355]	1.9	13.58	0.15	3.126
360	[0.355, 0.365]	1.9	13.65	0.15	3.230
370	[0.365, 0.375]	1.8	14.81	0.15	3.013
380	[0.375, 0.385]	1.8	13.73	0.15	3.052
390	[0.385, 0.395]	1.7	13.47	0.16	3.169
400	[0.395, 0.405]	1.7	13.43	0.15	3.002

Table 6. Selection cuts for the 4μ displaced channel for the considered DP masses. Column $m_{\mu\mu}$ contains the invariant mass selection cuts, and $\epsilon_{m_{\mu\mu}}$ the corresponding fraction of background events in that interval. Column ‘BFD’ shows the background free distance above which no displaced background events are observed for a detector resolution of $5\ \mu\text{m}$. Column ϵ_X lists the efficiencies of the cuts on the signal, and the last column, Max N_{sig} , shows the number of surviving displaced signal events at the BFD.

displacement is assigned to the muon pair which originates from the DP. To obtain the correct boost, the displacements are calculated on an event-by-event basis, following the DP exponential decay law, with laboratory frame decay length λ_X^{lab} . The displacement is then scaled according to the particle momenta as before.

In order to assess the experimental sensitivity in each search region we proceed as follows. In the first step, we reject all events in both background and signal samples where the relative distance between the (already paired) muon and antimuon in either the PV or SV is larger than the experimental resolution. This selection removes events with wrongly paired muon-antimuon which effectively do not originate from the same vertex. Secondly, we define the position of the PV and SV as the middle point between the paired muon and antimuon, then calculate the overall displacement as the relative distance between PV and SV. We identify the displacement threshold above which the number of background events drops below one, i.e. where the background is completely reducible and a background free analysis applies.

By construction, the determination of the end point of the distribution of background

events suffers from large statistical fluctuations. In order to reduce these fluctuations we repeat the assignment of random displacements to the background samples 10^4 times, and then consider the average distribution of events as function of their displacement. The end point of the distribution is obtained adopting a regression fitting method inspired by machine learning: we evaluate the number of surviving events above fixed multiples of the chosen resolution⁴, and fit the logarithm of this distribution using a quadratic polynomial. The parameters of the quadratic polynomial are obtained applying a linear regression algorithm, trained using a gradient descent minimiser with squared error cost function, and the optimised parameters are then used to estimate the distribution end point. This procedure is repeated for each search region, to obtain the background free thresholds for each simulated DP mass, and gives more accurate results than a direct exponential fit to the background distribution. The background free thresholds are reported in units of the detector resolution in column four of Tab. 6. It turns out that for the displayed mass range, they are almost constant. Only at higher masses, not displayed due to a loss of signal sensitivity, do the thresholds drop to smaller values as expected.

The fractions of signal events with displacement above the background free thresholds are given in the last column of Tab. 6. They are used to obtain the sensitivity contour as a function of mass m_X and the gauge coupling g_X , following the statistical analysis described in Sect. 4, and specifically applying Eq. 4.2. The resulting 95% CL exclusion contour, for an assumed vertex resolution of $5 \mu\text{m}$ and an integrated luminosity of 50 ab^{-1} , is displayed in Fig. 11 by the dashed dark blue line and will be discussed in section 6.

5.5 Signatures with tau leptons

Because of the underlying $L_\mu - L_\tau$ symmetry, processes involving the production of DPs in association with tau leptons, as in $e^+e^- \rightarrow \tau^+\tau^-X$, have a cross section proportional to g_X^2 , similar in magnitude to those discussed above involving muons (see Fig. 4 and Tab. 1). Analogous search channels for DP detection can be defined replacing muons with taus in the final state: di-tau plus missing energy, di-taus plus two muons, four taus prompt, and two taus plus two displaced muons. Tau leptons are not observable directly, but are detected reconstructing their decay products. Their decays necessarily include light tau neutrinos which carry away a part of the kinematic information in form of missing energy or momentum. Tau observables are therefore more ‘smeared out’ compared to the analogous muon channels and have smaller selection and identification efficiencies, which eventually leads to an overall lower sensitivity. Dedicated searches for light resonances decaying into tau pairs are being performed at Belle II [27], which provide the existing most stringent limits in this signature. Those constraints are however superseded by analogous analyses on signatures with muon final states.

For these reasons, in this study we do not further investigate the sensitivity of the Belle II detector to channels with tau leptons, but leave this for future work. Indeed, if a

⁴Since the simulated muon origins in the background sample were drawn from a Gaussian distribution which depends solely on the detector resolution, the end point of the distribution can be given in units of this resolution parameter.

positive signal would be discovered in any channel, signatures involving tau leptons could be decisive to fingerprint the underlying model.

6 Results

In this section we present our projections for the Belle II sensitivity on $L_\mu - L_\tau$ DPs in the search channels discussed above, assuming an integrated luminosity of 50 ab^{-1} . The exclusion limits derived through the analyses described above are displayed in Fig. 11 in the two dimensional parameter space of the model, scanning over the mass m_X and coupling g_X of the DP. For comparison, we report the most recent existing constraints from the collider experiments Belle II, BaBar, KLOE, CMS and LHCb, from the CCFR neutrino experiment, and indirect constraints from Fermilab measurements on the muon $g - 2$. Experimental analyses on general models, with an additional neutral vector boson connected to the SM through kinetic mixing ϵ are recast into our minimal $L_\mu - L_\tau$ framework using Eq. 2.2, i.e. dividing ϵ by the loop factor in Eq. 2.2 to obtain the gauge coupling g_X , while rescaling the excluded cross sections by the appropriate branching ratios.

Low mass region: Very light DPs, with mass below the di-muon threshold, can be probed only indirectly. In this mass region, the dominant exclusion limits are indeed given by the CCFR neutrino trident experiment, and by measurements of the muon $g - 2$ anomaly. The CCFR neutrino trident experiment studies the rare process $\nu N \rightarrow \nu \mu^+ \mu^-$, with the $\mu^+ \mu^-$ pair produced from muon-neutrino scattering off the Coulomb field of a nucleus. It is therefore particularly sensitive to additional contributions from neutral currents coupling to the muon flavour. At present, measurements on SM neutrino cross sections from CCFR [31] exclude gauge couplings above $g_X \simeq 10^{-3}$ for DP masses up to the di-muon threshold, and above $g_X \simeq 10^{-2}$ for DP masses of the order of 10 GeV (light grey shaded area of Fig. 11). The purple band indicates the parameter space which would explain, with 90% CL, the muon $g - 2$ discrepancy arising at the 4.2σ level from the comparison of the Run-1 measurements at FNAL [1] with the SM prediction from the Muon $g - 2$ Theory Initiative [7, 94–113]. As mentioned in the introduction, the size and significance of the discrepancy is currently not fully confirmed and the band should be taken as an indication only. The muon $g - 2$ constraints are mostly relevant in the low mass region, as is clear from Fig. 11. Constraints from collider experiments in this low mass region are only possible considering final states with missing energy or momentum. The exclusion limit from the Belle II analysis on the 2μ plus missing energy signature with an integrated luminosity dataset of 79.7 fb^{-1} [74] is represented by the solid light pink curve. For light DPs with masses below 1 GeV, it excludes gauge couplings above $g_X \simeq 3 \cdot 10^{-3}$, while for heavier DPs the sensitivity reduces exponentially to $g_X \simeq 1$ for masses of 8 GeV. Our optimised analysis on the 2μ plus missing energy channel (solid dark blue line), shows comparable sensitivity with respect to the current Belle II analysis, and it could test couplings above $g_X \simeq 3 \cdot 10^{-3}$ for DP masses up to 2 GeV, and above $g_X \simeq 10^{-1}$ for DP masses up to 8 GeV.

Two muon final states: Analyses on final states with only two muons are, in general, the least constraining. Searches for DPs at KLOE are sensitive to masses between 520 MeV

to 990 MeV, and include both decay modes into muon and pion pairs [60]. In the context of the $L_\mu - L_\tau$ model, only the former is relevant, and the contour obtained with an integrated luminosity of 1.93 fb^{-1} , represented by the solid purple line, excludes gauge couplings up to $g_X \simeq 5 \cdot 10^{-2}$. The dashed brown curve is derived from the CMS analysis on direct production of a light resonance decaying into a muon pair, with integrated luminosity of 96.6 fb^{-1} [18]. It uses a trigger selection and muon identification optimized for the low-mass region considered, and it is sensitive to DP masses between 1.1 GeV and 7.9 GeV, excluding the region between 2.6 and 4.2 GeV, i.e. around the J/Ψ , $\Psi(2S)$, and $\Upsilon(1S)$ resonances. It excludes gauge couplings as small as $g_X \simeq 2 \cdot 10^{-2}$ for very light DPs, with exponentially decreasing sensitivity to $g_X \simeq 1$ for heavier DPs. The LHCb analysis on light resonances decaying into a muon pair is obtained with a dataset corresponding to an integrated luminosity of 5.5 fb^{-1} [15]. Both prompt and displaced signatures are considered, and the exclusion limits are represented by the dashed black and solid black lines respectively. The LHCb prompt analysis shows a similar sensitivity to the analogous CMS one, but also covering the region below 1 GeV, down to the di-muon threshold, where it excludes gauge couplings $g_X \simeq 8 \cdot 10^{-3}$. In the mass region between the di-muon threshold and 300 MeV, the analysis with displaced signatures gives the best sensitivity, excluding gauge couplings down to $g_X \simeq 10^{-3}$. In comparison with these experimental results, we observe that our analysis on displaced DP decays (dashed dark blue curve) shows a shape similar to the analogous LHCb result, and a significantly improved sensitivity to gauge couplings below $g_X \simeq 10^{-4}$.

Four muon final states: Analyses on final states with 4 muons provide strong constraints in the $L_\mu - L_\tau$ model parameter space, especially for DP heavier than 1 GeV. The BaBar exclusion curve (solid orange line) has been obtained from the analysis of the 4μ prompt signature, considering the dataset corresponding to an integrated luminosity of 514 fb^{-1} , taken at the $\Upsilon(4S)$ resonance and in the neighborhood of the $\Upsilon(3S)$ and $\Upsilon(2S)$ peaks [23]. It covers the mass region above the di-muon threshold, excluding gauge couplings below $g_X \simeq 10^{-3}$ up to masses of 2 GeV, while for heavier DPs the sensitivity reduces exponentially to $g_X \simeq 1$ for masses of 8 GeV. An analogous analysis from Belle II with a dataset corresponding to an integrated luminosity of 643 fb^{-1} [25] shows a similar sensitivity (solid red line). Belle II performs slightly worse than BaBar for DP lighter than 2 GeV, while marginally improving BaBar exclusions for DPs heavier than 2 GeV. Very recently, an analysis of 178 fb^{-1} in the four muon final state has been released [114] by Belle II. The preliminary results (solid dark green line) show a sensitivity similar to BaBar and previous Belle II analyses, and further improving upon CCFR. The combination of all three results sets stringent exclusion limits for DP masses above 3 GeV. The CMS analysis of the four muons prompt final state with an integrated luminosity of 77.3 fb^{-1} [21] covers only DPs heavier than 5 GeV (solid brown line), and provides the strongest exclusion down to $g_X \simeq 5 \cdot 10^{-3}$. Our results on the four muons prompt signature (dot-dashed dark blue line) show a significant improvement with respect to BaBar and previous Belle II analyses, increasing the gauge coupling exclusion by roughly a factor 2. For DPs as heavy as 5-6 GeV, our analysis is sensitive to gauge couplings down to $g_X \simeq 5 \cdot 10^{-3}$, and comparable with the CMS high mass analysis.

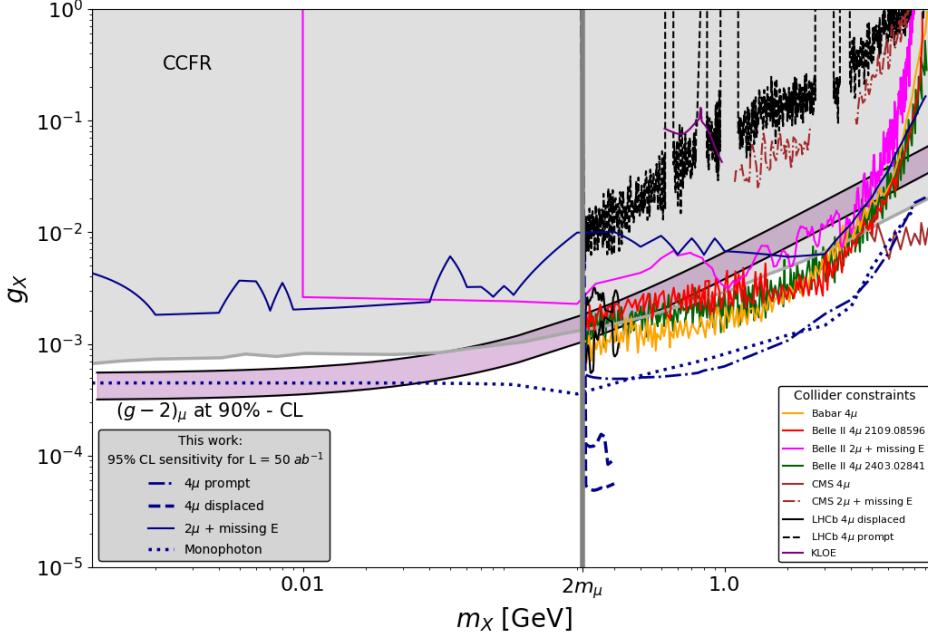


Figure 11. Summary of existing constraints and projected 95% CL sensitivities for Belle II with integrated luminosity of 50 ab^{-1} . Constraints across the whole energy range are provided by CCFR (solid light grey line), probing the neutrino trident production [31] and by Belle II, probing the $2\mu + \cancel{E}$ process (solid light pink line) [74]. Constraints that probe generic new light vector boson models are given by KLOE (solid purple line) [60] and CMS (dashed brown line) [18], both probing the $2\mu + \cancel{E}$ final state, and by LHCb (dashed black and solid black lines respectively) [15] with a search in the prompt and displaced 4μ channels; with values of ϵ being recast into the $U(1)_{L_\mu-L_\tau}$ model considered here. Other relevant constraints, in addition to CCFR, are given by Babar [23], Belle II [25, 114] and CMS [21], which look for resonances in the prompt 4μ channel. The purple band indicates the parameter range which would solve, at 90% confidence level, the 4.2σ muon $g-2$ discrepancy, see the text for further details.

A special mention is deserved by our study of the monophoton channel, whose sensitivity curve is given by the dotted dark blue line. The interpretation of this signature within the $L_\mu-L_\tau$ framework shows a remarkable potential for constraining specifically the minimal construction we have considered. The underlying process is indeed very sensitive to the kinetic mixing ϵ , which in our case is not a free parameter, but instead directly connected to the gauge coupling g_X through the kinetic mixing loop factor, $f(m_\mu, m_\tau, q)$. This analysis predicts the strongest sensitivity for DP masses below the di-muon threshold, excluding down to $g_X \simeq 4 \cdot 10^{-4}$, which is comparable or better than the strongest indirect bound from the muon $g-2$. For heavier DPs, the sensitivity of the monophoton analysis closely follows the one of the four muons prompt analysis.

7 Conclusions

In this work we have explored the sensitivity of the Belle II experiment on a minimal dark photon (DP) model with an underlying $L_\mu - L_\tau$ extra U(1) gauge group. Assuming the 50 ab^{-1} target luminosity of Belle II, we projected the sensitivity contours of multiple signatures on the model’s parameter space which, in its minimal configuration, reduces to the DP’s mass-coupling plane $m_X - g_X$. We considered the most promising signatures providing the best sensitivity at lepton colliders. They include final states where the DP appears as missing energy, such as the monophoton and two muons plus missing energy channels, and also multi-lepton final states where a pair of muons originates from the DP decay. The latter can arise as a prompt signature, i.e. as a resonant excess in a narrow invariant mass bin, or as a displaced signature, where the long-lived DP decays at a measurable distance with respect to the principal interaction point. For the analysis of this particular signature, we included the simulation of displaced decay events in both signal and background samples. In all the simulated events we considered the detector’s fiducial acceptance and reconstruction efficiencies for each particle, and for the VXD a resolution of $5 \mu\text{m}$ is assumed. The sensitivity projections are compared to the most recent results from direct searches of DPs at lepton colliders from the BaBar, Belle and KLOE experiments, at the LHC from the CMS and LHCb experiments, and to indirect probes using CCFR neutrino trident production data and the muon anomalous magnetic moment $g - 2$.

We find that with its ultimate 50 ab^{-1} target dataset, the Belle-II sensitivity on light DPs will improve on all existing exclusion limits. For very light DPs, i.e. below the two muon decay threshold, we observe the strongest sensitivity in the monophoton channel, which will overlap or extend the sensitivity band of the muon $g - 2$ indirect probe. When the DP is heavy enough to decay into a pair of muons, multi-leptonic final states will provide the most sensitive signatures, and only for heavy DPs ($m_X > 8 \text{ GeV}$) the LHC sensitivity becomes dominant.

The displaced decay signature in particular reveals a significant potential for the searches of narrow, long-lived DPs. Despite its limited sensitivity region, it allows to probe parameter regions not accessible through other signatures. The shape of the sensitivity contour is strongly dependent on the choice of the minimal VXD spacial resolution. In the minimal $L_\mu - L_\tau$ model, the typical DP decay displacements are indeed comparable with the VXD resolution. Assuming $5 \mu\text{m}$, we showed that the displaced analysis can test DP couplings $g_X \sim 10^{-4}$ and below, improving current bounds by one order of magnitude. While this assumption may seem optimistic, future developments in the muon track reconstruction may allow this level of precision or even better. In fact, even small further improvements of the VXD resolution would lead to critical reductions of the SM fake displaced background rates. This in turn would significantly increase the sensitivity of long-lived particles searches and eventually turn this signature into a very promising channel for the discovery of such BSM signals.

While $L_\mu - L_\tau$ DPs would also decay into tau pairs with a significant rate, we did not focus on signatures involving tau leptons, because the experimental challenges connected

to their reconstruction generally decrease the overall sensitivity in comparison with purely muonic final states. Yet, we stress that a combined fit of different search channels can help to identify the specific characteristics of the new physics model, such as an additional BSM symmetry group. For instance, the equivalence of DP decay rates into muons and taus would provide strong indications of an underlying $L_\mu - L_\tau$ symmetry. Similarly, assessing the BSM contribution to the monophoton channel gives a direct handle on the kinetic mixing parameter ϵ . This parameter is very sensitive to the presence of additional hidden states, and can help to distinguish between BSM models with extra gauged $U(1)_X$ symmetries and generic models featuring additional vector boson resonances.

The analysis methods presented in this work are very general and can be applied to various BSM scenarios across different collider experiments. The generic procedure, to determine for each signature the optimal kinematic cuts maximising the experimental sensitivity to a new physics signal, can be applied to different detector configurations and BSM models. In addition, our analysis of displaced signatures, which includes the simulation of both signal and background contributions, can be easily adapted to specific experimental environments and BSM constructions predicting long-lived particles. To fully assess the ultimate experimental sensitivity, more accurate theoretical predictions including higher order corrections and extra radiation are required, together with detailed detector simulations. While this level of analysis is beyond the scope of our current study, we plan to address some of these aspects in future work.

Acknowledgements

We thank Prof. Gianluca Inguglia for useful discussions on the Belle II detector. CB is supported by an STFC PGR studentship. JF and TT were supported by the STFC Consolidated Grant ST/T000988/1 and TT currently by ST/X000699/1. JF acknowledges financial support from ICSC – Centro Nazionale di Ricerca in High Performance Computing, Big Data and Quantum Computing, funded by the European Union – NextGenerationEU.

References

- [1] **Muon g-2** Collaboration, B. Abi et al., *Measurement of the Positive Muon Anomalous Magnetic Moment to 0.46 ppm*, *Phys. Rev. Lett.* **126** (2021), no. 14 141801, [[arXiv:2104.03281](#)].
- [2] **Muon g-2** Collaboration, D. P. Aguillard et al., *Measurement of the Positive Muon Anomalous Magnetic Moment to 0.20 ppm*, [arXiv:2308.06230](#).
- [3] **Muon g-2** Collaboration, D. P. Aguillard et al., *Detailed Report on the Measurement of the Positive Muon Anomalous Magnetic Moment to 0.20 ppm*, [arXiv:2402.15410](#).
- [4] **CDF** Collaboration, T. Aaltonen et al., *High-precision measurement of the W boson mass with the CDF II detector*, *Science* **376** (2022), no. 6589 170–176.
- [5] M. Bauer and P. Foldenauer, *Consistent Theory of Kinetic Mixing and the Higgs Low-Energy Theorem*, *Phys. Rev. Lett.* **129** (2022), no. 17 171801, [[arXiv:2207.00023](#)].

- [6] R. Essig, P. Schuster, and N. Toro, *Probing Dark Forces and Light Hidden Sectors at Low-Energy e^+e^- Colliders*, *Phys. Rev. D* **80** (2009) 015003, [[arXiv:0903.3941](#)].
- [7] T. Aoyama et al., *The anomalous magnetic moment of the muon in the Standard Model*, *Phys. Rept.* **887** (2020) 1–166, [[arXiv:2006.04822](#)].
- [8] G. Colangelo et al., *Prospects for precise predictions of a_μ in the Standard Model*, [arXiv:2203.15810](#).
- [9] **CMD-3** Collaboration, F. V. Ignatov et al., *Measurement of the $e^+e^- \rightarrow \pi^+\pi^-$ cross section from threshold to 1.2 GeV with the CMD-3 detector*, [arXiv:2302.08834](#).
- [10] **CMD-3** Collaboration, F. V. Ignatov et al., *Measurement of the pion formfactor with CMD-3 detector and its implication to the hadronic contribution to muon ($g-2$)*, [arXiv:2309.12910](#).
- [11] S. Borsanyi et al., *Leading hadronic contribution to the muon magnetic moment from lattice QCD*, *Nature* **593** (2021), no. 7857 51–55, [[arXiv:2002.12347](#)].
- [12] D. Curtin, R. Essig, S. Gori, and J. Shelton, *Illuminating Dark Photons with High-Energy Colliders*, *JHEP* **02** (2015) 157, [[arXiv:1412.0018](#)].
- [13] P. Ilten, Y. Soreq, M. Williams, and W. Xue, *Serendipity in dark photon searches*, *JHEP* **06** (2018) 004, [[arXiv:1801.04847](#)].
- [14] **LHCb** Collaboration, R. Aaij et al., *Search for Dark Photons Produced in 13 TeV pp Collisions*, *Phys. Rev. Lett.* **120** (2018), no. 6 061801, [[arXiv:1710.02867](#)].
- [15] **LHCb** Collaboration, R. Aaij et al., *Search for $A' \rightarrow \mu^+\mu^-$ Decays*, *Phys. Rev. Lett.* **124** (2020), no. 4 041801, [[arXiv:1910.06926](#)].
- [16] **ATLAS** Collaboration, G. Aad et al., *Search for light long-lived neutral particles produced in pp collisions at $\sqrt{s} = 13$ TeV and decaying into collimated leptons or light hadrons with the ATLAS detector*, *Eur. Phys. J. C* **80** (2020), no. 5 450, [[arXiv:1909.01246](#)].
- [17] **ATLAS** Collaboration, G. Aad et al., *Search for dark photons from Higgs boson decays via ZH production with a photon plus missing transverse momentum signature from pp collisions at $\sqrt{s} = 13$ TeV with the ATLAS detector*, *JHEP* **07** (2023) 133, [[arXiv:2212.09649](#)].
- [18] **CMS** Collaboration, A. Hayrapetyan et al., *Search for direct production of GeV-scale resonances decaying to a pair of muons in proton-proton collisions at $\sqrt{s} = 13$ TeV*, *JHEP* **12** (2023) 070, [[arXiv:2309.16003](#)].
- [19] **CMS** Collaboration, A. M. Sirunyan et al., *Search for dark photons in Higgs boson production via vector boson fusion in proton-proton collisions at $\sqrt{s} = 13$ TeV*, *JHEP* **03** (2021) 011, [[arXiv:2009.14009](#)].
- [20] **CMS** Collaboration, A. M. Sirunyan et al., *Search for dark photons in decays of Higgs bosons produced in association with Z bosons in proton-proton collisions at $\sqrt{s} = 13$ TeV*, *JHEP* **10** (2019) 139, [[arXiv:1908.02699](#)].
- [21] **CMS** Collaboration, A. M. Sirunyan et al., *Search for an $L_\mu - L_\tau$ gauge boson using $Z \rightarrow 4\mu$ events in proton-proton collisions at $\sqrt{s} = 13$ TeV*, *Phys. Lett. B* **792** (2019) 345–368, [[arXiv:1808.03684](#)].
- [22] **BaBar** Collaboration, J. P. Lees et al., *Search for a Dark Photon in e^+e^- Collisions at BaBar*, *Phys. Rev. Lett.* **113** (2014), no. 20 201801, [[arXiv:1406.2980](#)].

- [23] **BaBar** Collaboration, J. P. Lees et al., *Search for a muonic dark force at BABAR*, *Phys. Rev. D* **94** (2016), no. 1 011102, [[arXiv:1606.03501](#)].
- [24] **KLOE-2** Collaboration, D. Babusci et al., *Search for light vector boson production in $e^+e^- \rightarrow \mu^+\mu^-\gamma$ interactions with the KLOE experiment*, *Phys. Lett. B* **736** (2014) 459–464, [[arXiv:1404.7772](#)].
- [25] **Belle** Collaboration, T. Czank et al., *Search for $Z' \rightarrow \mu^+\mu^-$ in the $L\mu-L\tau$ gauge-symmetric model at Belle*, *Phys. Rev. D* **106** (2022), no. 1 012003, [[arXiv:2109.08596](#)].
- [26] K. Ban, Y. Jho, Y. Kwon, S. C. Park, S. Park, and P.-Y. Tseng, *Search for new light vector boson using J/Ψ at BESIII and Belle II*, *JHEP* **04** (2021) 091, [[arXiv:2012.04190](#)].
- [27] **Belle-II** Collaboration, I. Adachi et al., *Search for a $\tau^+\tau^-$ resonance in $e^+e^- \rightarrow \mu^+\mu^-\tau^+\tau^-$ events with the Belle II experiment*, *Phys. Rev. Lett.* **131** (2023), no. 12 121802, [[arXiv:2306.12294](#)].
- [28] **BaBar** Collaboration, J. P. Lees et al., *Search for Invisible Decays of a Dark Photon Produced in e^+e^- Collisions at BaBar*, *Phys. Rev. Lett.* **119** (2017), no. 13 131804, [[arXiv:1702.03327](#)].
- [29] B. Batell, R. Essig, and Z. Surujon, *Strong Constraints on Sub-GeV Dark Sectors from SLAC Beam Dump E137*, *Phys. Rev. Lett.* **113** (2014), no. 17 171802, [[arXiv:1406.2698](#)].
- [30] **NA64** Collaboration, D. Banerjee et al., *Search for invisible decays of sub-GeV dark photons in missing-energy events at the CERN SPS*, *Phys. Rev. Lett.* **118** (2017), no. 1 011802, [[arXiv:1610.02988](#)].
- [31] W. Altmannshofer, S. Gori, M. Pospelov, and I. Yavin, *Neutrino Trident Production: A Powerful Probe of New Physics with Neutrino Beams*, *Phys. Rev. Lett.* **113** (2014) 091801, [[arXiv:1406.2332](#)].
- [32] P. deNiverville, M. Pospelov, and A. Ritz, *Observing a light dark matter beam with neutrino experiments*, *Phys. Rev. D* **84** (2011) 075020, [[arXiv:1107.4580](#)].
- [33] **CHARM-II** Collaboration, D. Geiregat et al., *First observation of neutrino trident production*, *Phys. Lett. B* **245** (1990) 271–275.
- [34] **CCFR** Collaboration, S. R. Mishra et al., *Neutrino Tridents and W Z Interference*, *Phys. Rev. Lett.* **66** (1991) 3117–3120.
- [35] G. Bellini et al., *Precision measurement of the ^7Be solar neutrino interaction rate in Borexino*, *Phys. Rev. Lett.* **107** (2011) 141302, [[arXiv:1104.1816](#)].
- [36] R. Essig, A. Manalaysay, J. Mardon, P. Sorensen, and T. Volansky, *First Direct Detection Limits on sub-GeV Dark Matter from XENON10*, *Phys. Rev. Lett.* **109** (2012) 021301, [[arXiv:1206.2644](#)].
- [37] R. Essig, T. Volansky, and T.-T. Yu, *New Constraints and Prospects for sub-GeV Dark Matter Scattering off Electrons in Xenon*, *Phys. Rev. D* **96** (2017), no. 4 043017, [[arXiv:1703.00910](#)].
- [38] A. Aboubrahim, M. M. Altakach, M. Klasen, P. Nath, and Z.-Y. Wang, *Combined constraints on dark photons and discovery prospects at the LHC and the Forward Physics Facility*, [[arXiv:2212.01268](#)].
- [39] C. Giovanetti, M. Lisanti, H. Liu, and J. T. Ruderman, *Joint Cosmic Microwave*

Background and Big Bang Nucleosynthesis Constraints on Light Dark Sectors with Dark Radiation, *Phys. Rev. Lett.* **129** (2022), no. 2 021302, [[arXiv:2109.03246](#)].

- [40] A. Kamada, K. Kaneta, K. Yanagi, and H.-B. Yu, *Self-interacting dark matter and muon $g - 2$ in a gauged $U(1)_{L_\mu - L_\tau}$ model*, *JHEP* **06** (2018) 117, [[arXiv:1805.00651](#)].
- [41] M. Bauer, P. Foldenauer, and J. Jaeckel, *Hunting All the Hidden Photons*, *JHEP* **07** (2018) 094, [[arXiv:1803.05466](#)].
- [42] J. L. Feng, J. Smolinsky, and P. Tanedo, *Detecting dark matter through dark photons from the Sun: Charged particle signatures*, *Phys. Rev. D* **93** (2016), no. 11 115036, [[arXiv:1602.01465](#)]. [Erratum: *Phys.Rev.D* 96, 099903 (2017)].
- [43] **Fermi-LAT** Collaboration, M. Ackermann et al., *Searching for Dark Matter Annihilation from Milky Way Dwarf Spheroidal Galaxies with Six Years of Fermi Large Area Telescope Data*, *Phys. Rev. Lett.* **115** (2015), no. 23 231301, [[arXiv:1503.02641](#)].
- [44] **LHCb** Collaboration, R. Aaij et al., *Searches for low-mass dimuon resonances*, *JHEP* **10** (2020) 156, [[arXiv:2007.03923](#)].
- [45] L. Lee, C. Ohm, A. Soffer, and T.-T. Yu, *Collider Searches for Long-Lived Particles Beyond the Standard Model*, *Prog. Part. Nucl. Phys.* **106** (2019) 210–255, [[arXiv:1810.12602](#)]. [Erratum: *Prog.Part.Nucl.Phys.* 122, 103912 (2022)].
- [46] J. Alimena et al., *Searching for long-lived particles beyond the Standard Model at the Large Hadron Collider*, *J. Phys. G* **47** (2020), no. 9 090501, [[arXiv:1903.04497](#)].
- [47] E. Bernreuther, J. C. Mejia, F. Kahlhoefer, M. Krämer, and P. Tunney, *On the challenges of searching for GeV-scale long-lived particles at the LHC*, *JHEP* **04** (2021) 210, [[arXiv:2011.06604](#)].
- [48] S. N. Gninenko, N. V. Krasnikov, and V. A. Matveev, *Muon $g-2$ and searches for a new leptophobic sub-GeV dark boson in a missing-energy experiment at CERN*, *Phys. Rev. D* **91** (2015) 095015, [[arXiv:1412.1400](#)].
- [49] S. N. Gninenko and N. V. Krasnikov, *Probing the muon $g_\mu - 2$ anomaly, $L_\mu - L_\tau$ gauge boson and Dark Matter in dark photon experiments*, *Phys. Lett. B* **783** (2018) 24–28, [[arXiv:1801.10448](#)].
- [50] S. Gninenko, S. Kovalenko, S. Kuleshov, V. E. Lyubovitskij, and A. S. Zhevlakov, *Deep inelastic $e - \tau$ and $\mu - \tau$ conversion in the NA64 experiment at the CERN SPS*, *Phys. Rev. D* **98** (2018), no. 1 015007, [[arXiv:1804.05550](#)].
- [51] **NA48/2** Collaboration, J. R. Batley et al., *Search for the dark photon in π^0 decays*, *Phys. Lett. B* **746** (2015) 178–185, [[arXiv:1504.00607](#)].
- [52] I. Galon, D. Shih, and I. R. Wang, *Dark Photons and Displaced Vertices at the MUonE Experiment*, [[arXiv:2202.08843](#)].
- [53] J. L. Feng, I. Galon, F. Kling, and S. Trojanowski, *ForwArd Search ExpeRiment at the LHC*, *Phys. Rev. D* **97** (2018), no. 3 035001, [[arXiv:1708.09389](#)].
- [54] J. L. Feng, I. Galon, F. Kling, and S. Trojanowski, *Axionlike particles at FASER: The LHC as a photon beam dump*, *Phys. Rev. D* **98** (2018), no. 5 055021, [[arXiv:1806.02348](#)].
- [55] **FASER** Collaboration, A. Ariga et al., *FASER’s physics reach for long-lived particles*, *Phys. Rev. D* **99** (2019), no. 9 095011, [[arXiv:1811.12522](#)].

- [56] D. Curtin and M. E. Peskin, *Analysis of Long Lived Particle Decays with the MATHUSLA Detector*, *Phys. Rev. D* **97** (2018), no. 1 015006, [[arXiv:1705.06327](#)].
- [57] D. Curtin et al., *Long-Lived Particles at the Energy Frontier: The MATHUSLA Physics Case*, *Rept. Prog. Phys.* **82** (2019), no. 11 116201, [[arXiv:1806.07396](#)].
- [58] V. V. Gligorov, S. Knapen, M. Papucci, and D. J. Robinson, *Searching for Long-lived Particles: A Compact Detector for Exotics at LHCb*, *Phys. Rev. D* **97** (2018), no. 1 015023, [[arXiv:1708.09395](#)].
- [59] F. Bossi, *Dark Photon Searches Using Displaced Vertices at Low Energy e^+e^- Colliders*, *Adv. High Energy Phys.* **2014** (2014) 891820, [[arXiv:1310.8181](#)].
- [60] **KLOE-2** Collaboration, A. Anastasi et al., *Combined limit on the production of a light gauge boson decaying into $\mu^+\mu^-$ and $\pi^+\pi^-$* , *Phys. Lett. B* **784** (2018) 336–341, [[arXiv:1807.02691](#)].
- [61] **BaBar** Collaboration, J. P. Lees et al., *Search for Long-Lived Particles in e^+e^- Collisions*, *Phys. Rev. Lett.* **114** (2015), no. 17 171801, [[arXiv:1502.02580](#)].
- [62] **Belle-II** Collaboration, T. Abe et al., *Belle II Technical Design Report*, [arXiv:1011.0352](#).
- [63] M. Duerr, T. Ferber, C. Hearty, F. Kahlhoefer, K. Schmidt-Hoberg, and P. Tunney, *Invisible and displaced dark matter signatures at Belle II*, *JHEP* **02** (2020) 039, [[arXiv:1911.03176](#)].
- [64] M. Duerr, T. Ferber, C. Garcia-Cely, C. Hearty, and K. Schmidt-Hoberg, *Long-lived Dark Higgs and Inelastic Dark Matter at Belle II*, *JHEP* **04** (2021) 146, [[arXiv:2012.08595](#)].
- [65] E. Bernreuther, K. Böse, T. Ferber, C. Hearty, F. Kahlhoefer, A. Morandini, and K. Schmidt-Hoberg, *Forecasting dark showers at Belle II*, *JHEP* **12** (2022) 005, [[arXiv:2203.08824](#)].
- [66] T. Ferber, C. Garcia-Cely, and K. Schmidt-Hoberg, *BelleII sensitivity to long-lived dark photons*, *Phys. Lett. B* **833** (2022) 137373, [[arXiv:2202.03452](#)].
- [67] **Belle-II** Collaboration, I. Adachi et al., *Search for a long-lived spin-0 mediator in $b \rightarrow s$ transitions at the Belle II experiment*, [arXiv:2306.02830](#).
- [68] J. Heeck and W. Rodejohann, *Gauged $L_\mu - L_\tau$ Symmetry at the Electroweak Scale*, *Phys. Rev. D* **84** (2011) 075007, [[arXiv:1107.5238](#)].
- [69] K. S. Babu, C. F. Kolda, and J. March-Russell, *Implications of generalized Z - Z-prime mixing*, *Phys. Rev. D* **57** (1998) 6788–6792, [[hep-ph/9710441](#)].
- [70] **Particle Data Group** Collaboration, R. L. Workman et al., *Review of Particle Physics*, *PTEP* **2022** (2022) 083C01.
- [71] **Belle-II** Collaboration, W. Altmannshofer et al., *The Belle II Physics Book*, *PTEP* **2019** (2019), no. 12 123C01, [[arXiv:1808.10567](#)]. [Erratum: *PTEP* 2020, 029201 (2020)].
- [72] **Belle-II** Collaboration, V. Bertacchi, *Recent results from Belle II*, *Nucl. Part. Phys. Proc.* **324-329** (2023) 107–112.
- [73] **Belle-II** Collaboration, I. Adachi et al., *Search for an Invisibly Decaying Z' Boson at Belle II in $e^+e^- \rightarrow \mu^+\mu^-(e^\pm\mu^\mp)$ Plus Missing Energy Final States*, *Phys. Rev. Lett.* **124** (2020), no. 14 141801, [[arXiv:1912.11276](#)].
- [74] **Belle-II** Collaboration, I. Adachi et al., *Search for an invisible Z' in a final state with two muons and missing energy at Belle II*, [arXiv:2212.03066](#).

- [75] **Belle-II** Collaboration, G. De Pietro, *First data at Belle II and Dark Sector physics*, *PoS BEAUTY2018* (2018) 034, [[arXiv:1808.00776](#)].
- [76] **Belle II** Collaboration, M. Laurenza, *Dark-sector physics at Belle II*, *PoS PANIC2021* (2022) 047.
- [77] **BABAR** Collaboration, R. Godang, *Search for Muonic Dark Forces at BABAR*, *EPJ Web Conf.* **141** (2017) 02005, [[arXiv:1611.07934](#)].
- [78] N. D. Christensen and C. Duhr, *FeynRules - Feynman rules made easy*, *Comput. Phys. Commun.* **180** (2009) 1614–1641, [[arXiv:0806.4194](#)].
- [79] W. Kilian, T. Ohl, and J. Reuter, *WHIZARD: Simulating Multi-Particle Processes at LHC and ILC*, *Eur. Phys. J. C* **71** (2011) 1742, [[arXiv:0708.4233](#)].
- [80] M. Moretti, T. Ohl, and J. Reuter, *O’Mega: An Optimizing matrix element generator*, [hep-ph/0102195](#).
- [81] N. D. Christensen, C. Duhr, B. Fuks, J. Reuter, and C. Speckner, *Introducing an interface between WHIZARD and FeynRules*, *Eur. Phys. J. C* **72** (2012) 1990, [[arXiv:1010.3251](#)].
- [82] T. Ferber, A. Filimonova, R. Schäfer, and S. Westhoff, *Displaced or invisible? ALPs from B decays at Belle II*, [arXiv:2201.06580](#).
- [83] **Belle-II Framework Software Group** Collaboration, T. Kuhr, C. Pulvermacher, M. Ritter, T. Hauth, and N. Braun, *The Belle II Core Software*, *Comput. Softw. Big Sci.* **3** (2019), no. 1 1, [[arXiv:1809.04299](#)].
- [84] **Belle-II** Collaboration, F. Abudinén et al., *Measurements of branching fractions and CP-violating charge asymmetries in multibody charmless B decays reconstructed in 2019-2020 Belle II data*, [arXiv:2109.10807](#).
- [85] A. Abashian et al., *Muon identification in the Belle experiment at KEKB*, *Nucl. Instrum. Meth. A* **491** (2002), no. 1-2 69–82.
- [86] **Belle-II** Collaboration, F. Wemmer et al., *Photon Reconstruction in the Belle II Calorimeter Using Graph Neural Networks*, *Comput. Softw. Big Sci.* **7** (2023), no. 1 13, [[arXiv:2306.04179](#)].
- [87] H. Svidras, M. Röhrken, S. Wehle, and K. Tackmann, *Measurement of the data to mc ratio of photon reconstruction efficiency of the belle ii calorimeter using radiative muon pair events*, .
- [88] **Belle-II SVD** Collaboration, K. Adamczyk et al., *The Belle II silicon vertex detector assembly and mechanics*, *Nucl. Instrum. Meth. A* **845** (2017) 38–42.
- [89] **Belle-II SVD** Collaboration, K. Adamczyk et al., *The design, construction, operation and performance of the Belle II silicon vertex detector*, *JINST* **17** (2022), no. 11 P11042, [[arXiv:2201.09824](#)].
- [90] **Belle-II** Collaboration, C. Schwanda et al., *Performance of the Belle II Silicon Vertex Detector*, *PoS Vertex2019* (2020) 014.
- [91] P. Wieduwilt et al., *Performance of production modules of the Belle II pixel detector in a high-energy particle beam*, *Nucl. Instrum. Meth. A* **991** (2021) 164978, [[arXiv:2101.10107](#)].
- [92] R. K. Maiti, *Search for muonic dark force and performance studies of lepton identification at Belle II*. PhD thesis, Institut of High Energy Physics, Vienna, Tech. U., 2023.

- [93] **Belle-II SVD** Collaboration, Z. Wang et al., *The Silicon Vertex Detector of the Belle II experiment*, *Nucl. Instrum. Meth. A* **1061** (2024) 169131.
- [94] T. Aoyama, M. Hayakawa, T. Kinoshita, and M. Nio, *Complete Tenth-Order QED Contribution to the Muon $g - 2$* , *Phys. Rev. Lett.* **109** (2012) 111808, [[arXiv:1205.5370](#)].
- [95] T. Aoyama, T. Kinoshita, and M. Nio, *Theory of the Anomalous Magnetic Moment of the Electron*, *Atoms* **7** (2019), no. 1 28.
- [96] A. Czarnecki, W. J. Marciano, and A. Vainshtein, *Refinements in electroweak contributions to the muon anomalous magnetic moment*, *Phys. Rev.* **D67** (2003) 073006, [[hep-ph/0212229](#)]. [Erratum: *Phys. Rev.* **D73**, 119901 (2006)].
- [97] C. Gnendiger, D. Stöckinger, and H. Stöckinger-Kim, *The electroweak contributions to $(g - 2)_\mu$ after the Higgs boson mass measurement*, *Phys. Rev.* **D88** (2013) 053005, [[arXiv:1306.5546](#)].
- [98] M. Davier, A. Hoecker, B. Malaescu, and Z. Zhang, *Reevaluation of the hadronic vacuum polarisation contributions to the Standard Model predictions of the muon $g - 2$ and $\alpha(m_Z^2)$ using newest hadronic cross-section data*, *Eur. Phys. J.* **C77** (2017), no. 12 827, [[arXiv:1706.09436](#)].
- [99] A. Keshavarzi, D. Nomura, and T. Teubner, *Muon $g - 2$ and $\alpha(M_Z^2)$: a new data-based analysis*, *Phys. Rev.* **D97** (2018), no. 11 114025, [[arXiv:1802.02995](#)].
- [100] G. Colangelo, M. Hoferichter, and P. Stoffer, *Two-pion contribution to hadronic vacuum polarization*, *JHEP* **02** (2019) 006, [[arXiv:1810.00007](#)].
- [101] M. Hoferichter, B.-L. Hoid, and B. Kubis, *Three-pion contribution to hadronic vacuum polarization*, *JHEP* **08** (2019) 137, [[arXiv:1907.01556](#)].
- [102] M. Davier, A. Hoecker, B. Malaescu, and Z. Zhang, *A new evaluation of the hadronic vacuum polarisation contributions to the muon anomalous magnetic moment and to $\alpha(m_Z^2)$* , *Eur. Phys. J.* **C80** (2020), no. 3 241, [[arXiv:1908.00921](#)]. [Erratum: *Eur. Phys. J.* **C80**, 410 (2020)].
- [103] A. Keshavarzi, D. Nomura, and T. Teubner, *$g - 2$ of charged leptons, $\alpha(M_Z^2)$, and the hyperfine splitting of muonium*, *Phys. Rev. D* **101** (2020), no. 1 014029, [[arXiv:1911.00367](#)].
- [104] A. Kurz, T. Liu, P. Marquard, and M. Steinhauser, *Hadronic contribution to the muon anomalous magnetic moment to next-to-next-to-leading order*, *Phys. Lett.* **B734** (2014) 144–147, [[arXiv:1403.6400](#)].
- [105] K. Melnikov and A. Vainshtein, *Hadronic light-by-light scattering contribution to the muon anomalous magnetic moment revisited*, *Phys. Rev.* **D70** (2004) 113006, [[hep-ph/0312226](#)].
- [106] P. Masjuan and P. Sánchez-Puertas, *Pseudoscalar-pole contribution to the $(g_\mu - 2)$: a rational approach*, *Phys. Rev.* **D95** (2017), no. 5 054026, [[arXiv:1701.05829](#)].
- [107] G. Colangelo, M. Hoferichter, M. Procura, and P. Stoffer, *Dispersion relation for hadronic light-by-light scattering: two-pion contributions*, *JHEP* **04** (2017) 161, [[arXiv:1702.07347](#)].
- [108] M. Hoferichter, B.-L. Hoid, B. Kubis, S. Leupold, and S. P. Schneider, *Dispersion relation for hadronic light-by-light scattering: pion pole*, *JHEP* **10** (2018) 141, [[arXiv:1808.04823](#)].
- [109] A. Gérardin, H. B. Meyer, and A. Nyffeler, *Lattice calculation of the pion transition form*

- factor with $N_f = 2 + 1$ Wilson quarks, *Phys. Rev.* **D100** (2019), no. 3 034520, [[arXiv:1903.09471](#)].
- [110] J. Bijnens, N. Hermansson-Truedsson, and A. Rodríguez-Sánchez, *Short-distance constraints for the HLbL contribution to the muon anomalous magnetic moment*, *Phys. Lett.* **B798** (2019) 134994, [[arXiv:1908.03331](#)].
 - [111] G. Colangelo, F. Hagelstein, M. Hoferichter, L. Laub, and P. Stoffer, *Longitudinal short-distance constraints for the hadronic light-by-light contribution to $(g - 2)_\mu$ with large- N_c Regge models*, *JHEP* **03** (2020) 101, [[arXiv:1910.13432](#)].
 - [112] T. Blum, N. Christ, M. Hayakawa, T. Izubuchi, L. Jin, C. Jung, and C. Lehner, *The hadronic light-by-light scattering contribution to the muon anomalous magnetic moment from lattice QCD*, *Phys. Rev. Lett.* **124** (2020), no. 13 132002, [[arXiv:1911.08123](#)].
 - [113] G. Colangelo, M. Hoferichter, A. Nyffeler, M. Passera, and P. Stoffer, *Remarks on higher-order hadronic corrections to the muon $g - 2$* , *Phys. Lett.* **B735** (2014) 90–91, [[arXiv:1403.7512](#)].
 - [114] **Belle-II** Collaboration, I. Adachi et al., *Search for a $\mu^+\mu^-$ resonance in four-muon final states at Belle II*, [[arXiv:2403.02841](#)].